QUANTITY AND QUALITY OF GROUNDWATER DISCHARGE IN A HYPER-SALINE LAKE ENVIRONMENT, GREAT SALT LAKE, UTAH, USA

by

Richard Beau Anderson

A thesis submitted to the faculty of
The University of Utah
in partial fulfillment of the requirements for the degree of

Master of Science

in

Geology

Department of Geology and Geophysics

The University of Utah

December 2012

The University of Utah Graduate School

STATEMENT OF THESIS APPROVAL

The thesis of **Richard Beau Anderson**

has been approved by the following supervisory committee members:

Paul W. Jewell	, Chair	**6-30-2012** Date Approved
William P. Johnson	, Member	**6-30-2012** Date Approved
David L. Naftz	, Member	**6-30-2012** Date Approved

and by **D. Kip Solomon** , Chair of

the Department of **Geology and Geophysics**

and by Charles A. Wight, Dean of The Graduate School.

ABSTRACT

Previous studies in Great Salt Lake (GSL) suggest that unmeasured sources of selenium (Se) may enter the lake via groundwater discharge. A fiber-optic distributed temperature sensing (FO-DTS) survey was performed in the south arm of GSL during 2010 to identify near-shore areas of groundwater discharge. The FO-DTS data found there are consistent cold-water temperature anomalies with measured seepage rates between 0.01–2.37 cm/day. The CRP survey also identified three continuous layers in the subsurface: (1) a top conductive layer 2 m thick with resistivity of 0.5 ohm-m; (2) a middle 3-4 m thick resistive layer with resistivity about 4-5 ohm-m; and (3) a bottom conductive layer with a resistivity about 0.5-1 ohm-m. The middle layer is likely mirabilite ($Na_2SO_4 \cdot 10\ H_2O$), a hard impermeable salt, which appears to decrease in thickness in a W-NW direction towards the lake. Water-level observations indicate the aquifer is semiconfined and supports the CRP data showing a thinning or disappearance of the salt layer. The positive seepage suggests the mirabilite may not be as impermeable as it seems or the top 1 m of the sand above the hard salt layer is acting as a shallow aquifer which transmits shallow groundwater discharge. The R/Ra values in the groundwater are <1 and the tritium concentrations (1.2-2.0 TU) in the groundwater suggests the water has components of old and young groundwater. Geochemical modeling shows that mirabilite saturation index values for the groundwater samples were all slightly >0, indicating the water is at equilibrium with respect to mirabilite. The open

water of GSL along the south shoreline had Se concentrations (1.9 ug/L) 3-4 times higher than 4 open water sites in the south arm of GSL (0.5 µg/L) measured during a 2006-2008 study. Geochemical modeling was performed on a groundwater sample collected 2 km north of a mine tailings pond containing elevated arsenic (As) and low Se concentrations. The modeling results suggest that under reducing conditions, As-bearing minerals are mobilized while Se-bearing minerals will likely precipitate out of solution possibly explaining why the shallow groundwater below the hard salt layer have low concentrations of Se (0.9-2.3 µg/L).

TABLE OF CONTENTS

LIST OF FIGURES

LIST OF TABLES

ACKNOWLEDGMENTS

Funding for this work was provided by the Utah Division of Forestry, fire, and State Lands; Utah Division of Wildlife Resources; and the U.S. Geological Survey.

I would like to thank my thesis committee members, David L. Naftz and Paul W. Jewell for their help and support with data interpretation and suggestions for improvement. I would like to thank the following USGS personnel; Fred D. Day Lewis and Rory Henderson for their help and expertise with the geophysics side of this project, Don Rosenbery for his help with the seepage meters, and Jay Cedarberg for his help with the monitoring wells, Phil Gardner for his assistance with collection of dissolved gases and his insights, and Bert Stolp for his valuable insights as well. Also, I would like to thank Kip Solomon and Alan Rigby at the University of Utah dissolved gas laboratory. I would especially like to thank David L. Naftz for his willingness to allow me to be a part of this project and for his invaluable insight and encouragement throughout the project, as well as the Friends of Great Salt Lake and their assistance with funding the Doyle Stephens Scholarship. I would also like to thank my wife Christie for her love and support. Use of any manufacturers names in this report are used for identification purposes only and does not indicate endorsement by the U.S. Geological Survey or the University of Utah in any way.

INTRODUCTION

Groundwater discharge is an important component of the hydrologic and chemical cycles of limnological systems, yet it remains difficult to locate and quantify (Winter, 1981 and Hunt et al., 1996). Geophysical methods are often employed to help locate groundwater and understand subsurface conditions. Examples of these methods include electrical resistivity (Keller and Frischknecht, 1966), seismic refraction (Dorbin, 1976), and aerial thermal IR imagery (Palluconi and Meeks, 1985). These studies are often expensive and time consuming, therefore new cost effective techniques are being developed. One such technique is fiber-optic distributed temperature sensing (FO-DTS), an emerging technology with previous nonhydrologic applications in the petroleum, fire, and nuclear industries (Lane, 2007). Recently, fiber-optic technology has been applied to help identify areas of groundwater discharge and observe the spatial and temporal variations in groundwater at the freshwater-saltwater interface (Henderson et al., 2008). The study area is located in the south arm of Great Salt Lake (GSL), a hypersaline terminal lake in northwest Salt Lake Valley (Figure 1). Richardson (1906) conducted the first investigation of groundwater conditions in Salt Lake Valley and produced maps showing depth to ground water and areas of flowing wells. Taylor and Leggette (1949) conducted a more thorough investigation that included many well records, and discussions of groundwater occurrence, recharge, discharge, and chemical quality. Mower (1968) discussed groundwater discharge toward GSL in basin-fill deposits.

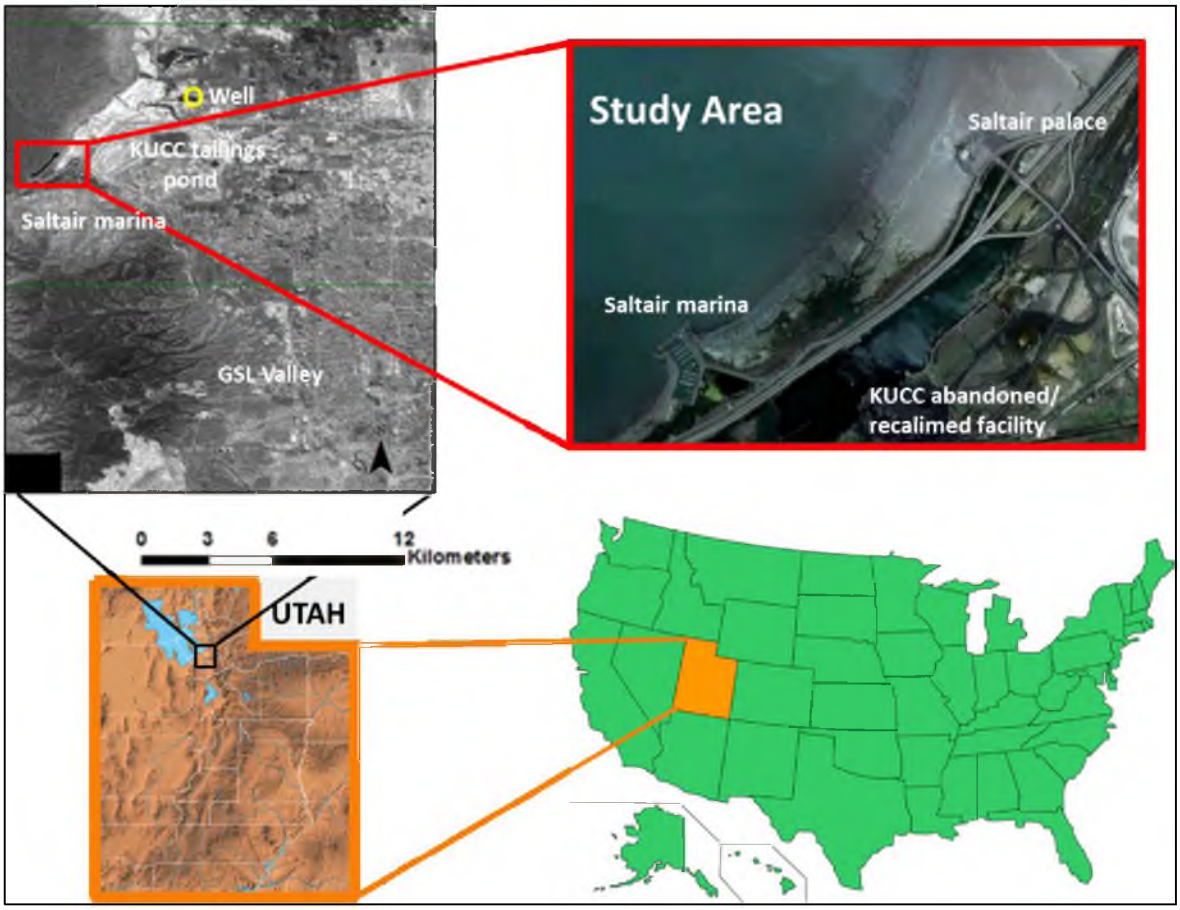

Figure 1: A map that shows the location of the study area that is found in the south arm of Great Salt Lake (GSL), Utah. Note the black line which depicts the area between the Saltair palace and GSL marina just north of the KUCC abandoned/reclaimed facility. Also present is Well 404704112060401 which is 2 km N of the KUCC tailings pond, and 9 km NW of the study area.

Arnow and Stephens (1975) estimated the groundwater inflow to GSL from 1931-1976. Herbert et al. (1985) conducted a seepage study of six canals in Salt Lake County. Waddell et al. (1987) evaluated the chemical quality of ground water in the basin-fill aquifer for the 1969–1985 time periods. Thiros (1992) compiled selected hydrologic data for Salt Lake Valley with emphasis on data from the shallow unconfined aquifer and confining layers. Anderson and Susong (1995) mapped groundwater recharge and discharge areas for the principal aquifers in Salt Lake Valley. Thiros (1995) investigated the chemical composition and movement of groundwater, and the hydrologic properties of basin-fill material, to better understand the flow system in Salt Lake Valley. Lambert (1995a) produced a three-dimensional, finite-difference, numerical groundwater flow model for the basin-fill aquifer, which he (Lambert, 1995b) subsequently used to produce capture zones for selected public supply wells. Stolp and Brooks (2009) studied the hydrology and simulated the groundwater flow in the Tooele Valley groundwater basin.

The vast majority of water entering GSL is by surface flow from three major rivers, the Bear, the Provo-Jordan, and the Weber, while additional inputs come from smaller tributaries, groundwater seepage and irrigation drainage water (Mohammed and Tarboton, 2011). Groundwater in the Salt Lake Valley generally moves from recharge areas near the mountain fronts toward the Jordan River and GSL. Groundwater moves upward in the discharge area through the confined aquifer, into and through overlying confining layers, and into the shallow unconfined aquifer, where it discharges to the Jordan River, to drains, by evapotranspiration, or minor seepage to GSL (Thiros et al., 2010). The minimal groundwater discharge to GSL is estimated between 75,000 – 1,200,000 acre-inch/year which is about 3% of the total annual inflow to the lake (Arnow

and Stephens, 1975).

Millions of migratory waterfowl and shorebirds utilize GSL as a source of food and rest during the migrating seasons (Caudell and Conover, 2006). GSL also supports a vibrant brine shrimp population that provides an important food source for migratory waterfowl (Aldrich and Paul, 2002). Brine shrimp cysts are harvested seasonally from GSL and used as a food source in aquaculture industries throughout the world (Bengston et al., 1991). The lake provides significant mineral resources (sodium and magnesium chloride, potassium salts, magnesium metal, and chlorine gas) vital to the economic well-being of the state, while also providing employment to thousands of Utahns (Roberts, 2010). GSL is a complex system that has been the subject of recent ecological studies (Stephens and Birdsey, 2002, Johnson et al. 2008, Naftz et al. 2008, Belovsky et al. 2011). Visitors utilize the lake for recreational purposes such as hunting, birding and sailing each year and preservation of this fragile and unique ecosystem depends on the quality and quantity of water entering the lake.

Despite the ecological and economic importance of GSL, little is known about the quantity or quality of groundwater discharging to the lake, therefore FO-DTS technology in the south arm of GSL may be useful in locating potential areas of groundwater discharge and to study the quality and source of the groundwater. Of recent note, the Jordan Valley Water Conservancy District is in the process of obtaining a permit to discharge byproduct water from reverse osmosis treated groundwater to the south shore of GSL (Shelley, 2010), which will input additional selenium (Se) and other heavy metal loads like arsenic (As) and mercury (Hg) into the lake. In response to increasing public concern regarding Se inputs to GSL ecosystem, the United States Geological Survey

(USGS) in collaboration with other agencies estimated Se loads entering GSL from six primary inflow sites from May 2006-March 2008 (Naftz et al., 2008). The investigation documented a net increase in Se concentrations, and indicated a substantial amount of unmeasured sources of Se (~1,500 kg/year) entering the south arm of GSL. Unmeasured sources of Se may come from groundwater discharge, unmeasured surface flows, diffusion from lake sediment pore water, poorly characterized Se exchange between the north and south arm, and possible wind-blown particulates (Naftz et al., 2008). In response to the hypothesis that nonsaline groundwater discharge may be contributing Se loads to GSL, a preliminary electrical resistivity survey in September 2007 detected a shallow higher-resistivity zone, indicating the presence of nonsaline groundwater, along the south shoreline of GSL in the vicinity of the Saltair marina (Figure 1). The location of this zone was used to guide the selection of areas for follow-up study.

The USGS has a well-established network monitoring the stream flow and water-quality of surface water inflow entering the lake (U.S. Geological Survey a, 2012); however there is not a well-established network in place to monitor the quantity or quality of groundwater entering the lake. A Utah state standard for tissue based Se in GSL is 12.5 mg/kg (Utah Gov, 2012). The Environmental Protection Agency and the state of Utah criterion for Se in freshwater systems is ~5.0 µg/L (Gaddis and Hornbeck, 2011). Kennecott Utah Copper Corporation (KUCC) studies from 2000 - 2002 recommended a water-quality standard for selenium in GSL of 27 µg/L (Brix et al. 2004). Previous work by KUCC identified an area 1.5 km south of the Saltair marina in the south arm of GSL with elevated Se concentrations ranging from 500 – 17,000 µg/L in groundwater beneath the KUCC refinery (Figure 1) (KUCC, 1999). Modeling this

contaminant plume in the subsurface suggests minimal discharge to GSL; however, no groundwater monitoring data have been collected beneath GSL to verify the groundwater modeling results (Naftz et al., 2008).

In order for future planners to establish an accurate water budget for GSL and verify KUCC findings, the amount of groundwater discharge to the lake needs to be quantified. In addition, the source (s) of groundwater reaching GSL is important to current and future management decisions. For example, it is critical to determine if groundwater reaching the lake was recharged recently (< 50 years) or long ago (> 1000 years), because recently recharged water is generally more susceptible to contamination from anthropogenic compounds (Wright et al., 2004). In addition, the recharge elevation of groundwater is important in delineating recharge areas that need to be protected, as well as identifying likely groundwater flow paths to GSL. The objectives of this paper are to (1) locate potential areas of groundwater discharge beneath GSL with FO-DTS and continuous resistivity profile (CRP) technology; (2) quantify the amount of groundwater discharge with seepage meters based on the results from objective 1 and; (3) collect water samples and use dissolved gas concentrations, environmental isotopes, and water-quality data to determine the age, potential recharge elevation, evolution, and quality of groundwater entering GSL.

FIELD METHODOLOGY

Fiber-optic distributed temperature survey (FO-DTS)

The FO-DTS method involves sending a laser light along a fiber-optic cable which uses Raman back scatter to estimate temperature. Raman scattering is produced by inelastic collisions of photons with atoms or molecules within the fiber-optic cable. If a photon loses energy to the fiber, the scattered wavelength is longer (stokes signal); if a scattered photon gains energy from interactions, its energy is larger and therefore its wavelength is shorter (antistokes signal). The antistokes (energy gaining) is strongly temperature dependent, but the stokes signal is relatively independent of the temperature of the colliding molecule (Maher, 2006). By calculating a ratio of the antistokes to stokes signal intensities, an accurate temperature measurement can be obtained. Combining this temperature measurement technique with distance measurement through time-of-flight of light, the FO-DTS provides temperature measurements incrementally along the entire length of the fiber-optic cable (Moffett, 2008).

The use of temperature measurements to monitor areas of groundwater discharge relies on the temperature contrast between groundwater and surface water. Groundwater temperature is relatively stable year round and surface water temperature changes daily and seasonally, therefore groundwater discharge is relatively warm in the winter and cool in the summer (Smith, 2005). This relatively new FO-DTS technology can produce temperature time series data along the full length of a fiber-optic cable extending up to

10s of kilometers providing spatial resolution of about 1 meter, temporal resolution on the order of seconds to minutes, and temperature precision of about 0.1- 0.01 °C (Lane, 2007).

A FO-DTS survey was conducted along the south arm of GSL between the Saltair marina and the Saltair Palace. A 2 km yellow colored fiber-optic cable was spliced with a less robust black colored, 1 km fiber-optic cable which was deployed and arranged parallel to the lake shore June 8-10, 2010 (Figure 2). The fiber-optic cable was deployed by walking the cable out and pulling it along the shore while arranging it on the beach. After beach deployment, the cable was then moved into the water and placed onto the lake bed and anchored with bricks at about 30 m intervals zip-tied to the fiber-optic cable. Global positioning system (GPS) location, length along the cable, and water depth were recorded at all locations. Temperature data were collected every 20 minutes at approximately 1 meter intervals from June 11 to July 13, 2010, except during a period from June 17-23 when a storm severed the connection and only the first 2 km of the yellow cable was active. Once the black cable was respliced with the yellow cable it was repositioned (Figure 2). The FO-DTS system was configured and operated by a Sensortran DTS 5100 unit housed in a trailer at Saltair marina and the data were wirelessly transmitted and stored in a Dropbox account.

Fiber-optic systems yield relative measurements of temperature which must be calibrated to produce absolute measurements. The calibration step corrects raw temperature output by the instrument to match independently measured temperatures at various locations along the fiber-optic cable. An initial calibration was performed by the Sensortran instrument software. This software calibration is developed during cable

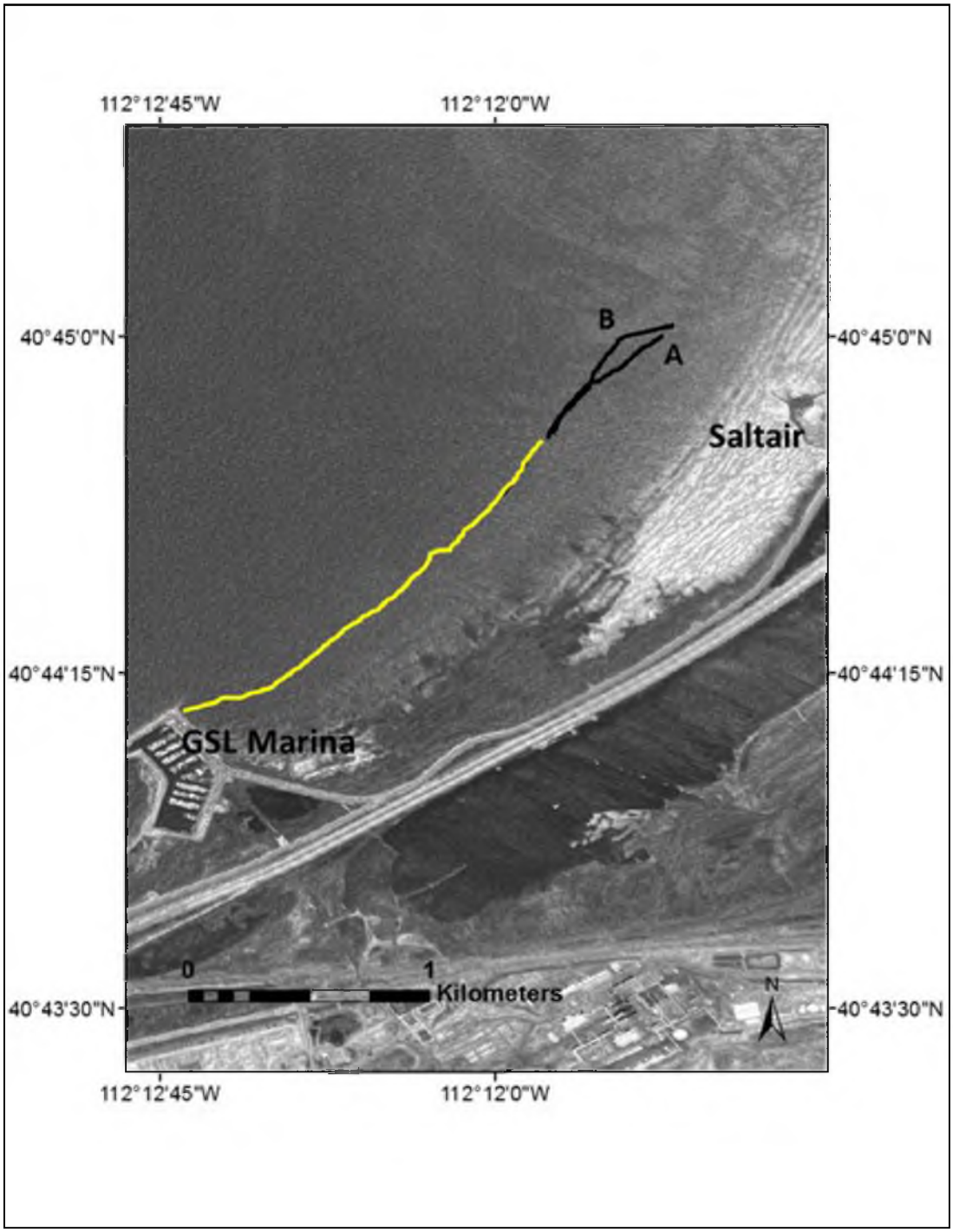

Figure 2: A map that shows the study area and the location of the fiber-optic distributed temperature sensing (FO-DTS) cable trace which is a total of 3 km long. The yellow trace is the first 2 km's and the black trace is the last 1 km depicting the trace before the storm (A) and where the cable was positioned after the storm (B).

configuration and is static in the sense that the parameters of the calibration do not change in time. Field experience using FO-DTS and changes in environmental conditions at the instrument (e.g., large changes in air temperature) or on the cable (e.g., physical strain) can affect measurements and degrade the effectiveness of the static calibration. A dynamic calibration is performed to correct the temperature time series output by the instrument in a manner accounting for changes to the instrument or cable over time. In static calibration, the parameters defining the calibration formula are identified only once, and calibration data are only a snapshot of temperature. In dynamic calibration, the parameters defining the calibration are updated continuously using temperature time series for calibration data. Calibration data are provided by Hobo TidBit thermistors at three locations along the cable: (1) an ice bath in the trailer near the Sensortan instrument, (2) an ice bath along the cable, located at a splice between the two cable segments, and (3) an ice bath at a location near the end of the cable.

The goal of calibration is to correct raw temperature, $T_{raw}(x_i, t_j)$, at each cable measurement location x_i and every measurement time, t_j, to match independently measured data at a subset of locations. The form of calibration is somewhat arbitrary, and many approaches are possible, e.g., offset corrections, scaling corrections, and gain corrections (linear or polynomial), and various combinations of these in space and (or) time. For this study, a calibration is assumed of the form:

$$T_{cal}(x_i, t_j) = T_{raw}(x_i, t_j) + C_{offset}(t_j) + C_{scale} \cdot T_{raw}(x_i, t_j) + C_{gain} \cdot (x_i - x_0) \quad (1)$$

where,

$T_{cal}(x_i, t_j)$ is the calibrated temperature;

$C_{offset}(t_j)$ is an offset correction which varies in time;

C_{scale} is a temperature-scaling correction;

C_{gain} is the coefficient of a linear gain correction in space; and

x_0 is the location of the first calibration point.

Calibration coefficients ($C_{offset}(t_j)$, C_{scale}, and C_{gain}) are found by solving a multivariate linear regression problem to minimize the differences between predicted (calibrated) and observed temperatures at the calibration baths. Thus, we seek to identify the calibration coefficients to transform raw to calibrated data, minimizing the sum of squared errors where we have observations:

$$E = \sum_{j=1}^{ntimes}\left[T_{cal}(x_{bath\_1}, t_j) - T_{bath\_1}(t_j)\right]^2 + \left[T_{cal}(x_{bath\_2}, t_j) - T_{bath\_2}(t_j)\right]^2 \quad (2)$$

Equation 2 assumes calibration to observed temperature from baths at two locations: $T_{bath\_1}(t_j)$ and $T_{bath\_2}(t_j)$. Equation 1 is thus applied separately to the two segments of cable, i.e., segment A (yellow cable) from the instrument bath to the splice bath, and segment B (black cable) from the splice bath to the bath at the end of the cable. For segment A, x_0 is set to the location of the bath near the instrument, and for segment B, x_0 is set to the location of the bath at the splice. Regression was performed using Matlab. The raw and calibrated data, respectively, are compared to temperature observations at the three baths (Figure 3).

Current resistivity profile (CRP)

CRP surveys were used to map subsurface electrical resistivity to distinguish fresh from saline groundwater in shallow sedimentary units (Cross et al., 2006, 2008).

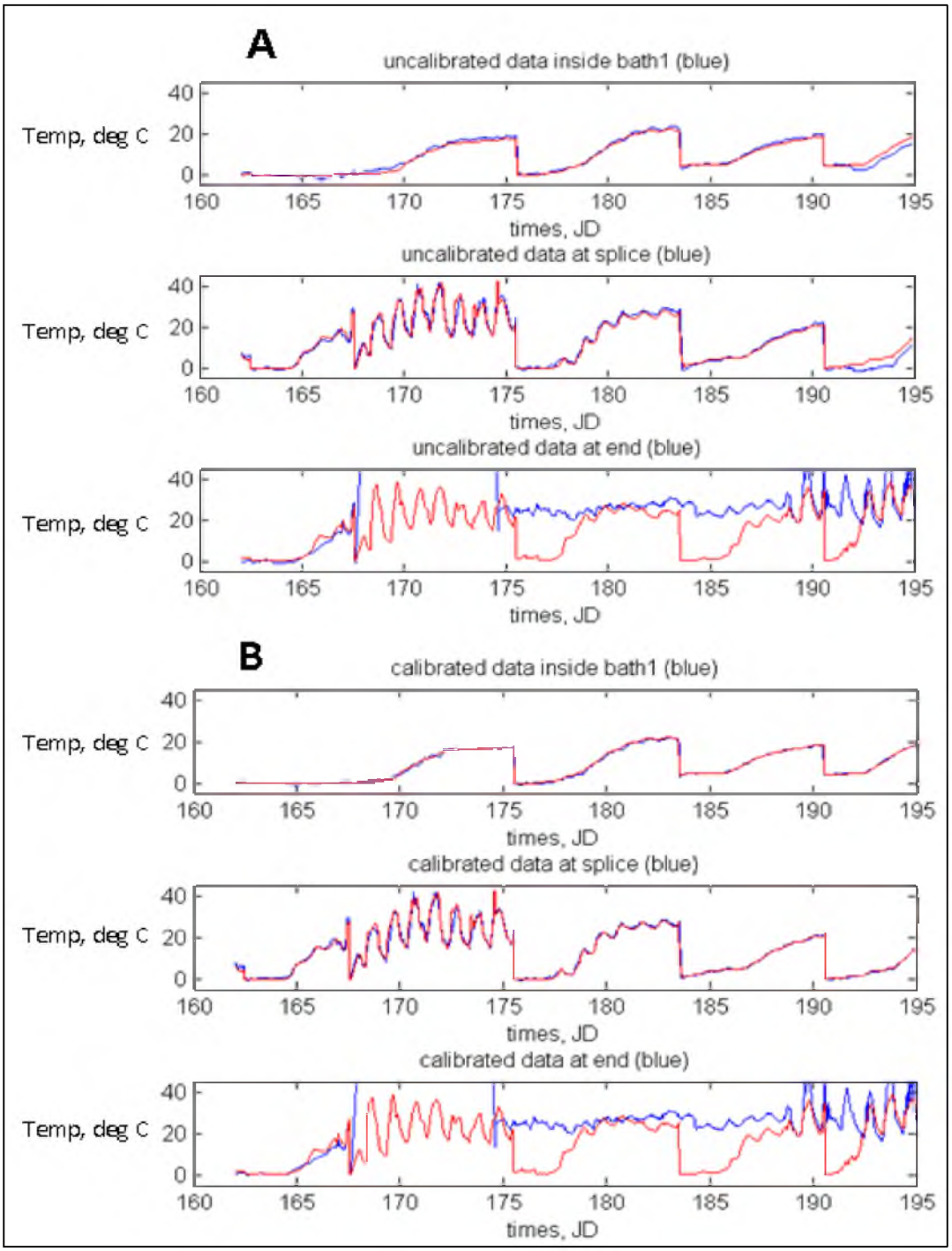

Figure 3: Graphs of the temperature data depicting the fiber-optic cable temperatures (blue) vs. the ice bath temperatures (red) during the julian days (JD) from June 11 – July 13, 2010. Graph A shows the uncalibrated data, while Graph B shows the calibrated data. Note how well the ice bath temperatures (red) and the fiber-optic temperatures (blue) line up on the calibrated graph and how bad the plots line up in the 3rd ice bath (data at end) due to the Hobo TidBit being compromised.

Resistivity is a function of lithology and pore fluid (Day-Lewis et al., 2006). Floating electrodes were towed behind a boat, and voltages collected continuously for various pairs of electrodes while current was applied between a fixed pair of electrodes. GPS data were collected concurrently with resistivity measurements to georeference the geophysical results. Bathymetry data also were collected using a depth finder to develop water-layer constraints for inverse modeling. In general, finer-grained consolidated materials are less electrically resistive than coarse unconsolidated materials or rock, and resistivity decreases with pore-fluid salinity and porosity (Hersir and Knútur, 2010).

In June 2010, the USGS collected CRP data in the south arm of GSL using an 8-channel Advanced Geosciences Inc. (AGI) super sting control unit and 11 electrode cables with interelectrode spacings of 5 m and 3 m, respectively. The goal was to noninvasively characterize subsurface structure and delineate possible zones of freshwater discharge to the lake. CRP data were collected along 14 tracks (Figure 4) near the Saltair marina with approximately 50 line km of electrical data collected shown as lines a – d.

Resistivity data were processed and inverse modeled in the commercially available software Res2DInv. Inverse modeling involves solving a nonlinear regression problem to produce the model of subsurface resistivity matching the field data to within experimental error; this procedure generates two-dimensional (2D) vertical cross sections of the electrical resistivity along boat tracks. The estimated resistivities are considered spatial averages and may poorly approximate true earth resistivity especially at depth where CRP sensitivity is lowest. Although quantitative interpretation of tomograms (i.e., conversion to estimates of pore-fluid salinity) would require additional modeling and

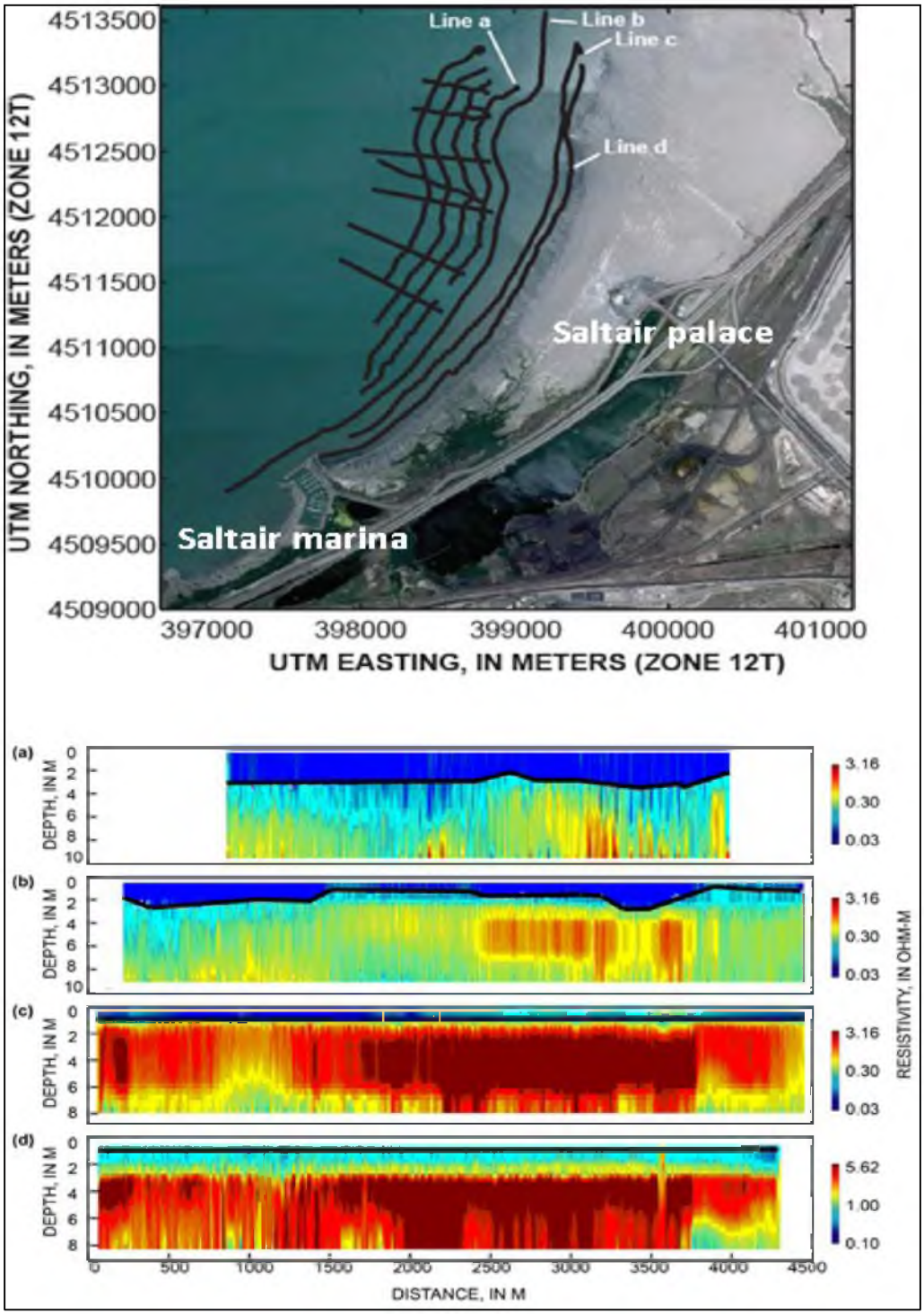

Figure 4: A map showing the approximate location of the boat tracks which were followed to collect continuous resistivity profile (CRP) data between the Saltair palace and GSL marina area, Great Salt Lake, Utah. Shore-perpendicular tomograms from the Saltair marina area, tomogram (d) is closest to shore, and (a) is farthest. The lake bottom is indicated by a solid black line.

work, the tomograms can qualitatively be used to indicate patterns of geologic structure, lithology, and (or) hydrologic processes such as groundwater resistivity.

Seepage meters

The flow of water at the interface between the overlying surface water and the aquifer represents the magnitude of seepage flux and is commonly measured directly through seepage meters. Relatively inexpensive meters are based on a simple concept and were initially developed in the 1940s to measure loss of water from irrigation canals (Israelson and Reeve , 1944) and have since been used in numerous studies of seepage fluxes in rivers and large lakes (Cherkauer and McBride, 1988) where current and scour are generally small. The basic concept of a seepage meter is to cover and isolate part of the sediment-water interface with a chamber open at the base and to measure the change in the volume of water contained in a bag attached to the chamber over a measured time interval.

The seepage flux (q) is calculated as:

$$q = \frac{(V_f - V_o)}{tA} \quad (3)$$

where V_f is the final volume of water in the bag, V_o is the initial volume of water in the bag, t is the time elapsed between when the bag was connected and disconnected, and A is the surface area of the chamber. Additional water in the bag represents positive (gaining) seepage and water loss from the bag represents downward (losing) seepage. One disadvantage to using the seepage meter is that they only effectively measure seepage flux at a point in space over a specific time interval.

Seventeen standard half-barrel seepage meters (Lee, 1977) were installed in the near-shore of the south arm of GSL near the Saltair marina (Figure 5). The seepage meters were made from plastic storage drums and plastic lids with diameters ranging from 32-59 cm cut in half and inverted. Total heights ranged from 10-25 cm. They were constructed with small holes drilled in the top to allow water to freely pass through in response to volume change (Boyle, 1994). Seepage meters were installed in the fine oolitic sand lake bottom by gently rotating the meters back and forth into the sediment to a depth of 10-15 cm below the sediment/water interface. The seepage meters were installed in water depths ranging from a few cm to 1.5 m. Attached to the cylinders were shelters made from commercially available clear plastic boxes, slightly larger than a full seepage bag (Figure 5). The plastic seepage bags had a total volume of 3.2 L and were attached to the seepage cylinder with female garden hose fittings. Lake sediments were placed inside the bag shelter as an anchor and a lid was placed on top to limit any pressure on the seepage bag caused by wave action (Rosenberry, 2008). Seepage bags included a shut-off valve that was opened and closed at precise times to allow accurate seepage measurements. Seepage was measured and recorded about twice a day during the week of August 8-15, 2010, by measuring the volume of water in the bag that has seeped into or out of it. This was done by pouring the water from the seepage bags into a 1 L plastic graduated cylinder. The deeper depths were accessed using mask and snorkel, while the shallow depths were accessed by foot. Careful attention was given to avoid disturbing the

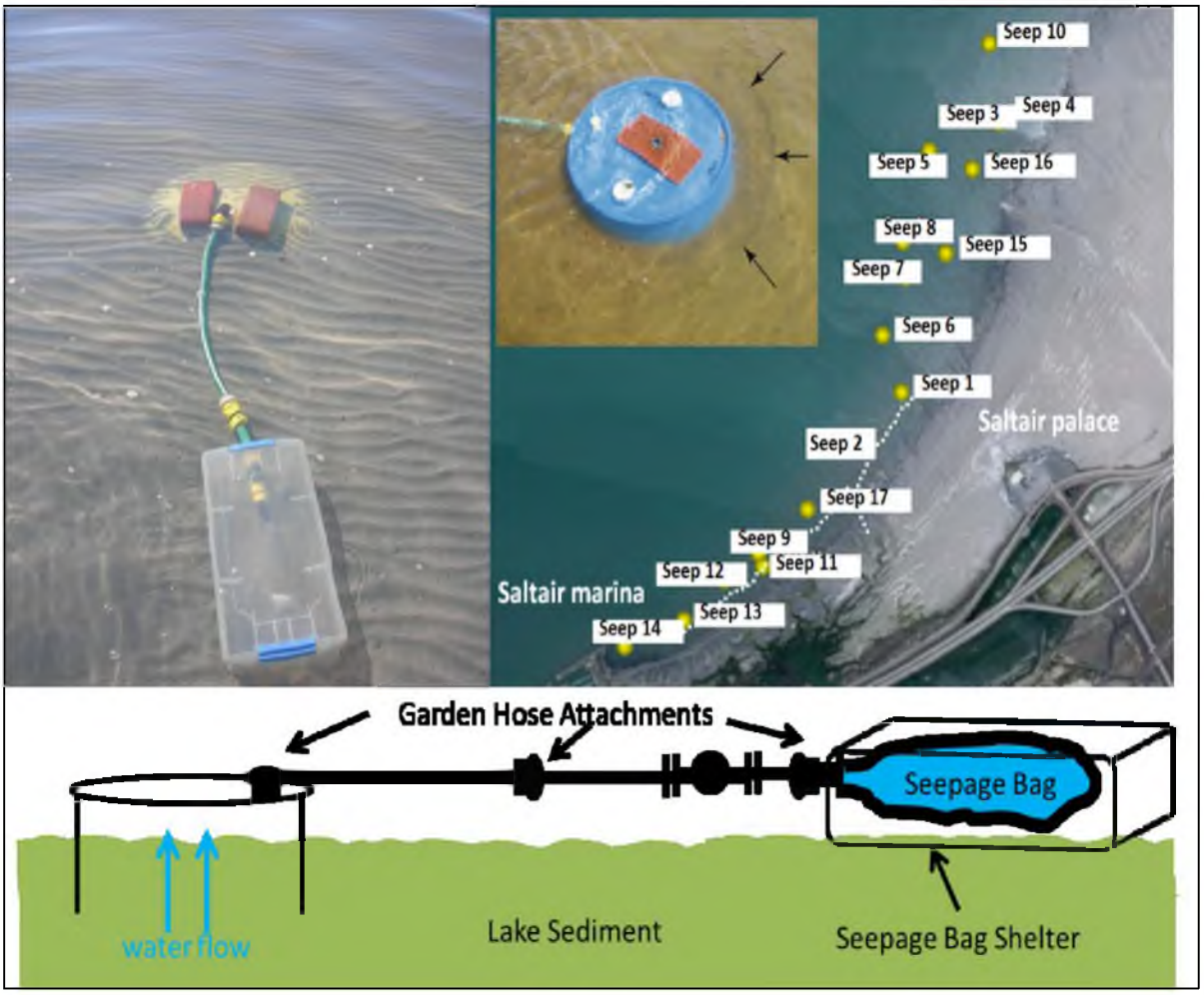

Figure 5: The location map and a photo of the seepage meters that were installed during the summer of 2010 to measure groundwater discharge in the near-shore of the south arm of GSL. Also a schematic cross-section of the meters installed in the lake sediment. Note the snap-on lid placed over the seepage bag and shelter to minimize wave action over the bag chamber.

sediments around each of the seepage meters to minimize sediment compaction that could artificially influence measured seepage rates.

Monitoring wells

Each of the well sites was chosen based on positive discharge recorded from the seepage meters, as well as taking into account the ease with which the geoprobe could access the sites and drill without the lake water being too deep for drill rig access. The drill rig was not able to access some of the sites due to water depth at the time of drilling, so the sites are considered an approximate location to seepage meter locations. A track mounted Geoprobe 6620 DT direct push drill rig was used to install seven shallow monitoring wells (Figure 6) and penetrate the hard salt layer in the near-shore of the Saltair beach (PVC pipe with a 2.5 cm outside diameter and 15.2 cm slotted interval) during November 2010. Upon completion of the monitoring wells each well was purged to remove the fine sediments from around the slotted interval using precleaned tygon tubing. During the purging process each well was pumped dry with the exception of Well 15 No. 3 which had higher recovery rates. Two of the wells (Well No.1 and Well 15 No.3) were drilled deep enough to penetrate the salt layer, while the remaining wells were not. A nonvented In-Situ, 15 PSI miniTROLL pressure transducer was installed in Well 15 No. 3 to measure the water-level every 15 minutes from early January to late April 2011. The transducer was checked monthly to download data and manually measure the water-level.

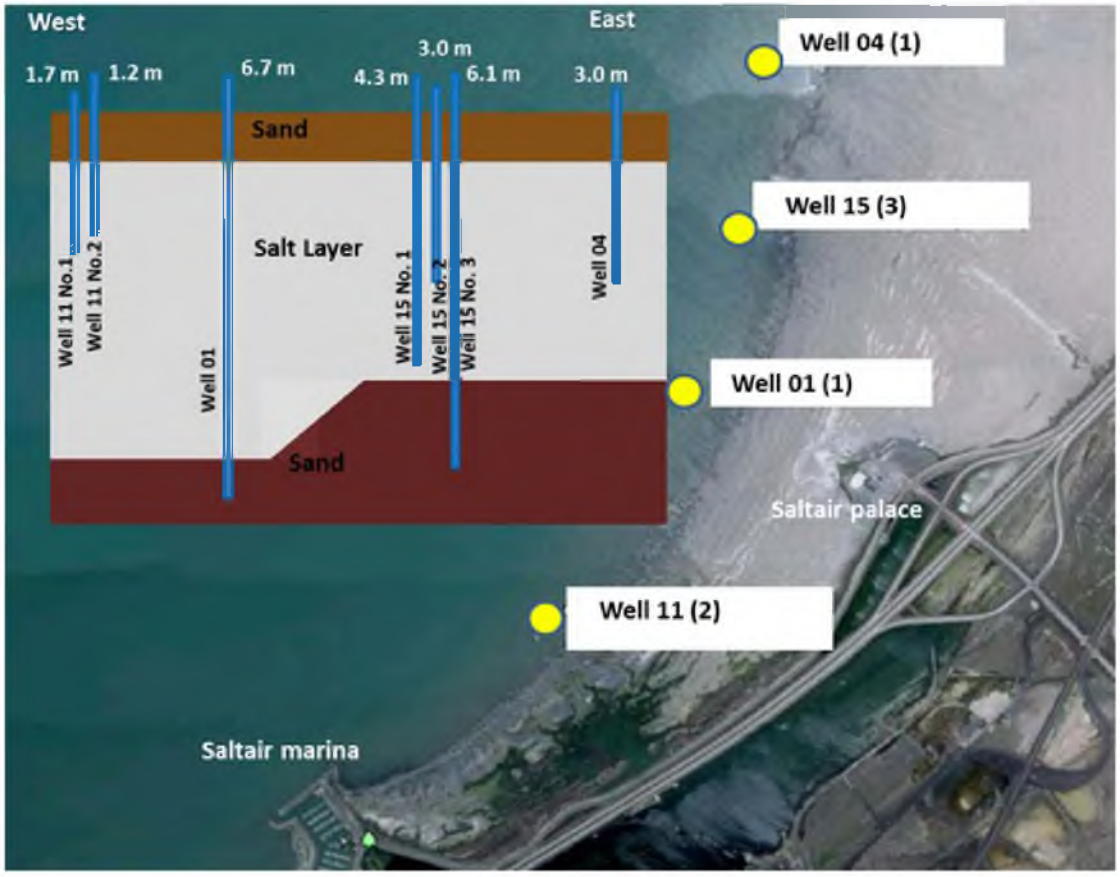

Figure 6: A cross-section that depicts each of the monitoring wells in relation to the salt layer and showing their corresponding total depths. Each of the seven monitoring wells (PVC pipe with a 2.5 cm outside diameter and 15.2 cm slotted interval) corresponds to a location found on the map which shows how many wells are present at each location.

Water sampling

Field parameters (pH, specific conductance, water temperature, dissolved oxygen, and oxidation-reduction potential) were measured with a calibrated In Situ Troll 9500 multiparameter water-quality probe from unfiltered water samples on site. The water was pumped through Masterflex tubing (Tubing ID 4.8 mm) at a rate of ~ 0.5 L/min using a Geotech Peristalitic Geopump connected to a flow through chamber attached to the Troll 9500 to ensure the water was not exposed to the atmosphere during measurement of field parameters. Sulfide concentrations in filtered (< 0.45 μm capsule filter) water samples were measured in the field using a colorimetric methylene-blue indicator method using a Hach Model 2010 spectrophotometer following Hach Method 376.2 (U.S. Environmental Protection Agency, 1983). Water samples were collected from each of the seven monitoring wells, along with samples from three surface water sites (two freshwater inflows and one open water sample of GSL water near Well 15); each site had a precleaned and dedicated tygon sampling tube to prevent inter-well contamination. Purge volumes were generally < two casing volumes due to the low yield of select monitoring wells; therefore, the wells were pumped until all the water was removed from the casing and then allowed to recover before samples were collected and processed. Standard USGS protocols were used for water-quality sampling (U.S. Geological Survey, 2012b). Filtered (< 0.45 μm capsule filter) and unfiltered water samples were collected with the clean hands/dirty hands techniques and other standard USGS protocol. Filtered (< 0.45 μm capsule filter) samples were collected in 250 mL polyethylene bottles for major cations which were then acidified to a pH of < 2 with 2 mL of 7.7N nitric acid and filtered nonacidified samples were collected in 250 mL polyethylene bottles for major

anions. Filtered (< 0.45 μm capsule filter) samples were collected in 250 mL glass bottles for both Hg and Se (preserved with 2 mL of 7.7N nitric acid), while 2 mL 1:1 omnitrace hydrochloric acid was added to preserve the samples. Unfiltered samples were collected in 125 mL glass bottles with polyseal caps for deuterium (δD) and oxygen-18 ($\delta^{18}O$) as well as analysis of tritium in the water. Filtered (< 0.45 μm capsule filter) samples were collected in 1 L polyethylene bottles for analysis of sulfur-34 ($\delta^{34}S$) and Oxygen-18 ($\delta^{18}O$) of sulfate in 1 L polyethylene bottles, a 15 cm long mirabilite core was collected for analysis of sulfur-34 ($\delta^{34}S$) and Oxygen-18 ($\delta^{18}O$) of sulfate as well. Immediately after collection the $\delta^{34}S$ sample was purged with air to remove H_2S (g).

Dissolved gases in groundwater were collected from the two deeper monitoring wells (Well 11 No. 1 and Well 15 No. 3) using advanced diffusion samplers which exchange gases over a semipermeable membrane developed by Gardner and Solomon (2009). The samplers were attached to tygon tubing and then gently lowered down each well and retrieved after being submersed for 24 hours to ensure that the gases dissolved in the groundwater had equilibrated with the gaseous volume inside the diffusion samplers. The samplers were then retrieved by attaching a hand operated bike pump which closes the intake valves, while the gas exchange piston is pushed forward, moving a slide valve which isolates the gas inlet port from the sample volume without affecting the total sample volume (Gardner and Solomon, 2009). The samplers were then removed from the wells and sealed using refrigeration clamps. Dissolved gases were also collected from Well 15 No. 3 using the copper tube extraction techniques described by Stute and Schlosser (2001). The sample was collected by connecting 30.5 cm length of 1-cm diameter copper tubing to tygon tubing and then gently lowering it down to the bottom of

the well while allowing the water to flow upwards into the sampler. Flow was then temporarily reversed using a peristaltic pump to close a check valve installed at the bottom of the copper tubing and trap water in the tubing until it could be sealed with refrigeration clamps. Care was taken to ensure that the sample was bubble-free and did not come into contact with the atmosphere, thus creating a representative sample of the dissolved gases in the groundwater.

LABORATORY METHODOLOGY

Samples

Laboratory analysis of $\delta^{34}S_{sulfate}$ was done by rinsing the sample with KCl. $BaCl_2$ then was added to the sample to precipitate $BaSO_4$, by adding 250 mL of sample, acidifing to a pH of about 4 with 1N HCl, and adding $BaCl_2$ to precipitate the sulfate from solution as $BaSO_4$. The precipitate was then filtered and rinsed with deionized water.

The major cation concentrations were measured by inductively coupled plasma-atomic emission spectrometry (ICP-AES) (Fishman, 1993) at the USGS National Water Quality Laboratory (NWQL), in Lakewood, CO. The major anion concentrations were measured with ion-selective electrode (ISE) (Fishman and Friedman, 1989) and ion-exchange chromatography (IC) (Fishman and Friedman, 1989) at the USGS NWQL, in Lakewood, CO. Dissolved Se concentrations were measured by inductively coupled plasma dynamic reaction cell-mass spectrometry (ICPDRC-MS) at Applied Speciation and Consulting, LLC, Inc. in Bothell, Washington. Total Hg concentrations were measured by cold vapor atomic fluorescence spectroscopy (CVAFS) (Garbarino and Damrau, 2001) at the USGS NWQL, in Lakewood, CO. Hydrogen and oxygen isotope concentrations in water were measured by mass spectrometry (MS) (Révész and Coplen, 2008a; Révész and Coplen, 2008b) and sulfur and oxygen isotope concentrations in dissolved sulfate were measured by continuous flow isotope-ratio mass spectrometry

(IRMS) (Révész and Qi, 2006) both at the USGS Stable Isotope Laboratory, Reston, VA. Tritium concentrations were measured by electrolytic enrichment and gas counting at the University of Miami Tritium Laboratory, Miami, FL. Stable isotope abundances are reported in parts per thousand (per mil) which are expressed as the ratio of the two most abundant isotopes in the sample compared to the same ratio in an international standard, using the 'delta' (δ) notation. The dissolved gas concentrations were measured by quadrupole and magnetic sector field mass spectrometry at the University of Utah Dissolved and Noble Gas Laboratory, SLC, UT.

A field process blank, matrix spike, matrix spike duplicate, and a matrix duplicate sample were collected on December 14, 2010 and analyzed for Se for quality-assurance and quality-control to assess contamination during sample collection, processing, and analysis. The blank was processed by pumping inorganic blank water, certified by the USGS NWQL through tygon tubing and other sampling equipment with a geotech peristalitic geopump. The samples were collected with the clean hands/dirty hands techniques and other standard USGS protocols as outlined in the water sampling section. The Se concentration in the process blank did not exceed the lower reporting limit (0.03 µg/L) in the sample; therefore, no Se contamination greater than the lower reporting limit was introduced during sample processing. Recovery of the matrix spike and the matrix duplicate was 111.7 and 118.0 %, which is within the accepted range of 75-125 %. The matrix duplicate sample was within 0.01 ug/L of the original sample.

Geochemical modeling

The saturation indices (SI) for mirabilite were calculated for the groundwater samples with PHREEQC Interactive using the PITZER thermodynamic database (Plummer et al., 1988). The SI of a salt in an aqueous solution is defined as log (IAP/K_{sp}), where IAP is the ion activity product and K_{sp} is the equilibrium constant of solubility product. $SI = 0$ there is equilibrium, $SI > 0$ indicates supersaturation, and $SI < 0$ subsaturation. PHREEQC-PITZ uses ion association and Pitzer expressions to account for the nonideality of aqueous solutions.

HYDROLOGY RESULTS AND DISCUSSION

Fiber-optic distributed temperature survey (FO-DTS)

Thousands of temperatures were recorded along the fiber-optic cable during the DTS 2010 study. Therefore, to best deal with these large data sets a mean daily temperature was calculated for the random days of June 18, 22-25, 27, and July 3, 10 (Figure 7). The temperature data sets are archived at the USGS and provided as supporting information for this article in the Appendix.

By plotting the mean temperature for each day and showing the standard deviation for each daily mean value a measure of how much variation or dispersion was obtained. Any value more than 2 standard deviations below the daily mean temperature is referred to as a cold-water temperature anomaly, which signifies possible groundwater discharge. Cold-water temperature anomalies persisting for more than 2 days at a time were observed in ~10 different locations along the fiber-optic cable near the Saltair marina during the summer of 2010 (Figure 8). The cold-water temperature anomalies are located mostly along the northeastern half of the fiber-optic cable assemblage. In contrast, very few cold-water temperature anomalies near the Saltair marina were found along the southwesterly end of the fiber-optic cable assemblage. The anomalies found at the NE half of the fiber-optic cable assemblage may be explained by the wetlands which are found in this area. In the middle of the study area which coincides with the NE half of the fiber-optic cable, small freshwater inflows enter the lake which are likely surface

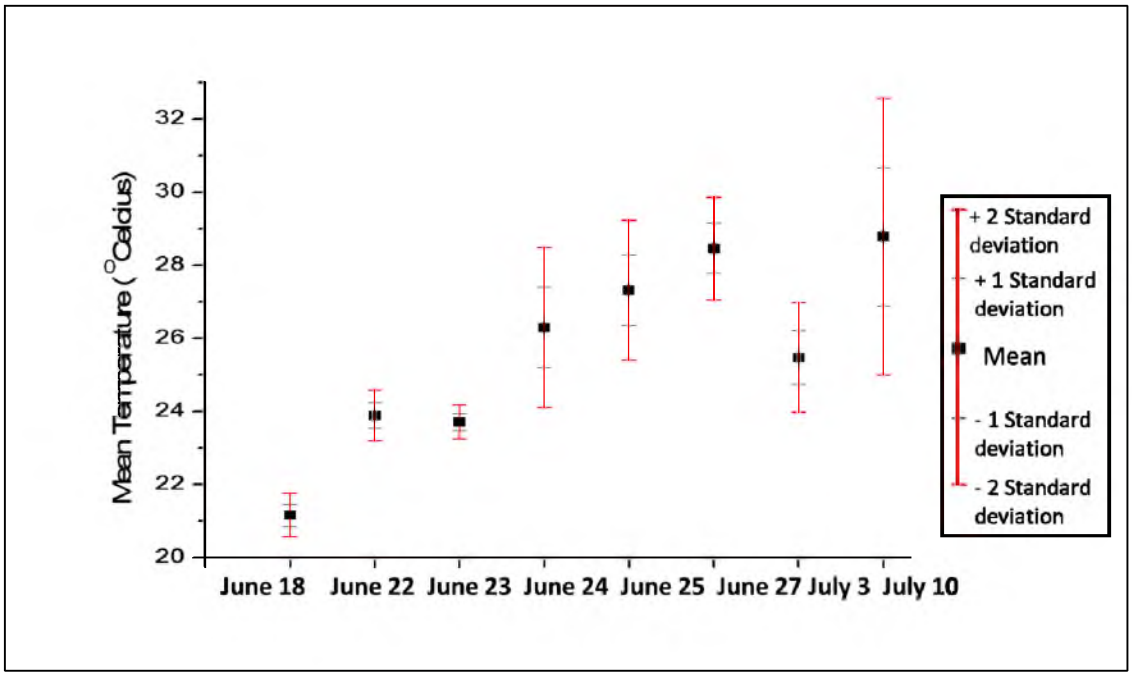

Figure 7: Mean daily temperatures and standard deviations were calculated for the following days during June – July, 2010. Note any temperature which is 2 standard deviations below the daily mean reflect cold-water temperature anomalies which may be potential groundwater discharge.

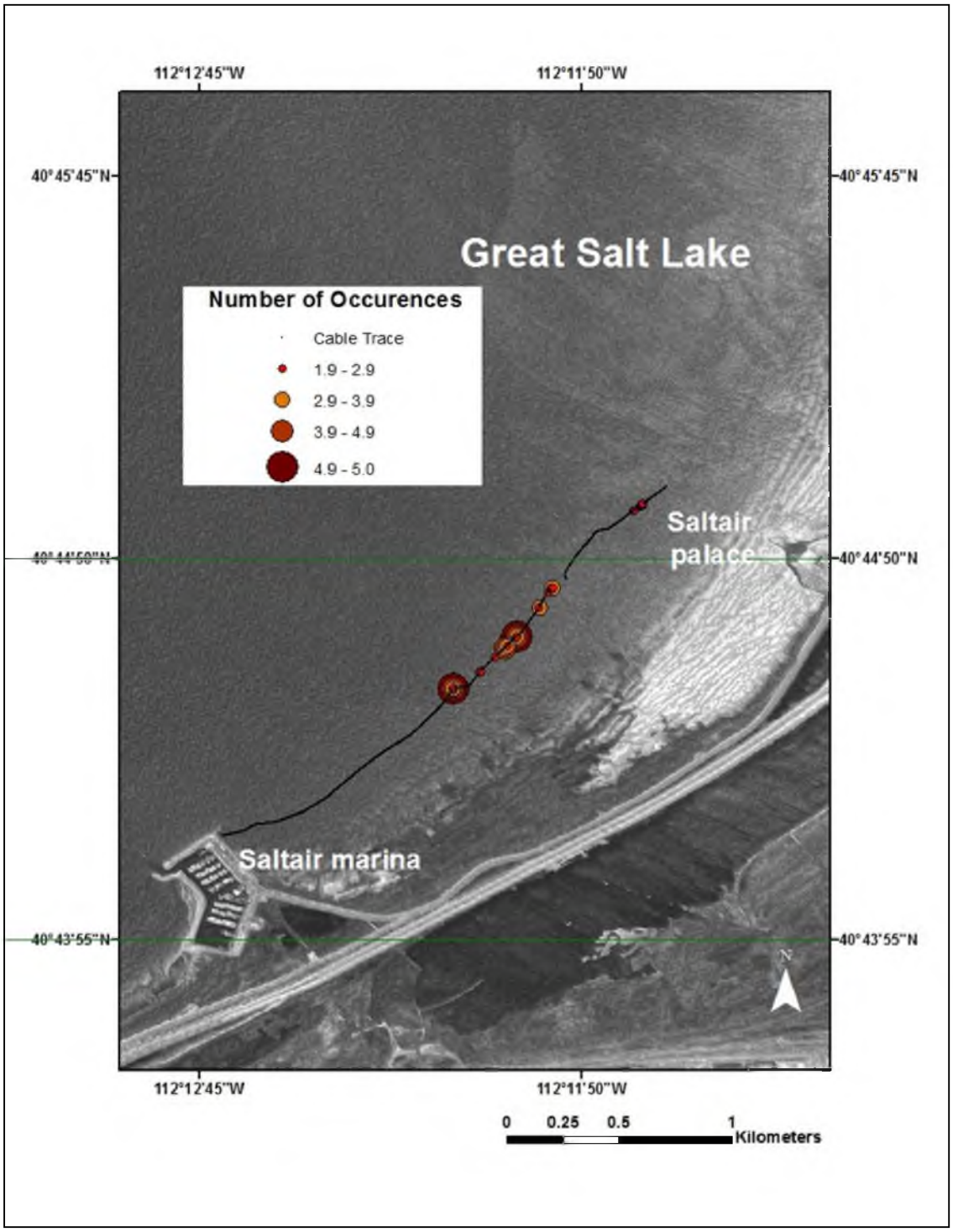

Figure 8: Cold-water temperature anomalous zones depicting the location and frequency of anomalies from June 11 to July 13, 2010.

expressions of groundwater seeps. These cold-water temperature anomalous zones are confirmed in the tomograms (Figures 9-11) which show the temperatures recorded along every meter of both the black and yellow cables for a 24- hour time period. The individual tomograms give insight into how long the cold-water temperature anomalies continue during the day. For example, on June 22 along meter marks 1500, 1550, and 1750, there are persistent low temperatures observed between 0300 to 1000 MDT (mountain daylight time) (Figure 9). These cold-water temperature anomalies are also shown in Figure 8 near the 2nd large, dark brown circle depicting an area of consistent cold-water temperature anomalies persisting for more than 4 days.

Less frequent cold-water temperature anomalies along the fiber-optic cable were also observed; however, less persistent anomalies were considered insignificant in comparison to cold-water temperature anomalies persisting for more than a few days. More frequent anomalies were assumed to be related to greater groundwater discharge than the anomalies which have fewer occurrences. Cold-water temperature anomalies observed in the tomograms and fiber-optic cable traces were used as guides to place the seepage meters to measure groundwater discharge in the near shore of the Saltair beach.

Current resistivity profile (CRP)

Data quality was good and inversions matched data within root-mean squared errors between 5 and 10 %. Representative tomograms near the Saltair marina show spatial variations both parallel and perpendicular to the lake shore (Figure 4). For the parallel profile nearest the shore (line d), the tomogram indicates three continuous layers. In order of increasing depth below the surface water sediment interface, they are: (1) a

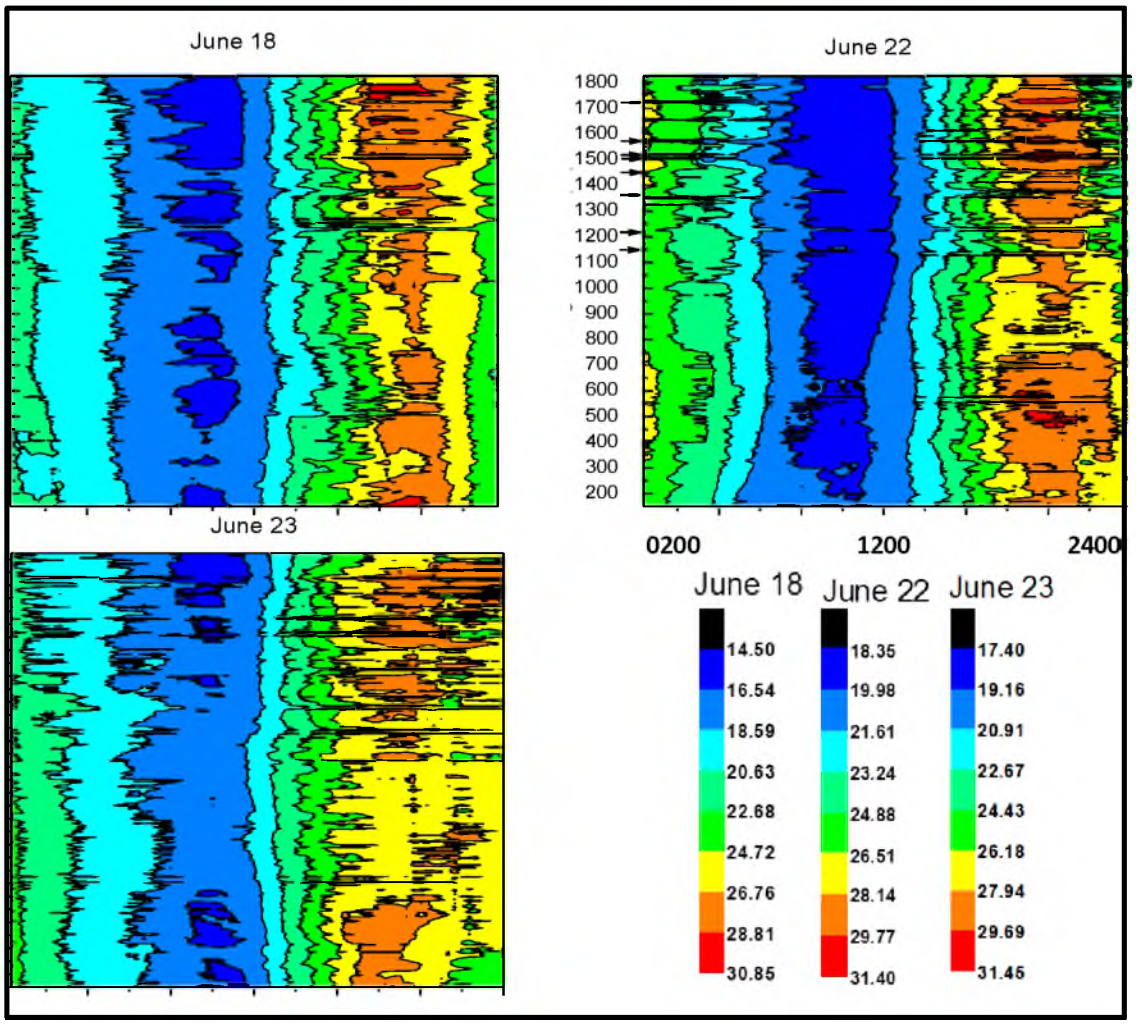
June 18
June 22
June 23
1800
1700
1600
1500
1400
1300
1200
1100
1000
900
800
700
600
500
400
300
200
0200
1200
2400
June 18
June 22
June 23
14.50
16.54
18.59
20.63
22.68
24.72
26.76
28.81
30.85
18.35
19.98
21.61
23.24
24.88
26.51
28.14
29.77
31.40
17.40
19.16
20.91
22.67
24.43
26.18
27.94
29.69
31.45

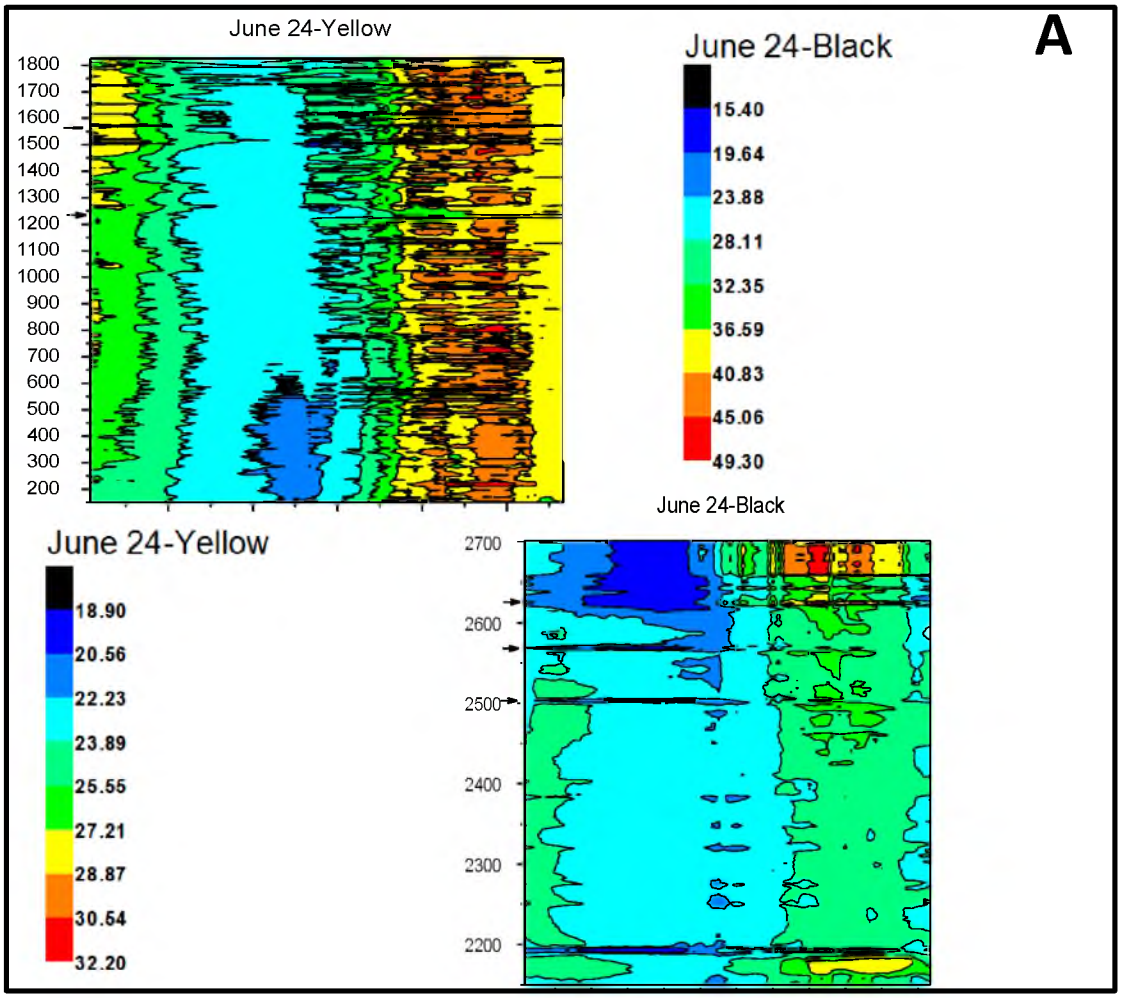

Figure 10: Graphs showing the distributed temperature sensing (DTS) data that were collected during the summer of 2010. These temperature profiles show black arrows where cold temperatures look to persist throughout the day. Each tomogram depicts temperatures in degrees celsius, and the time is MDT (mountain daylight time).

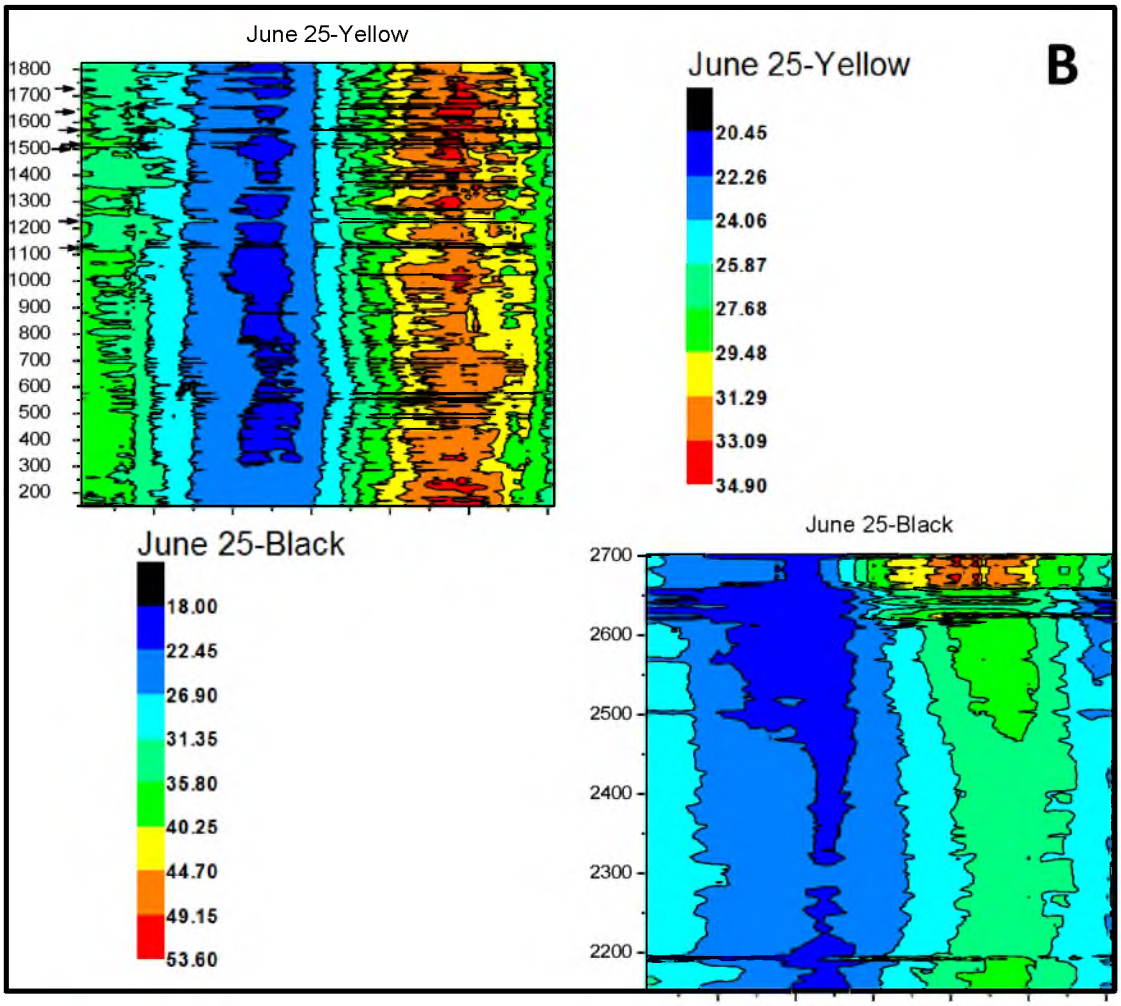

Figure 10 Continued:

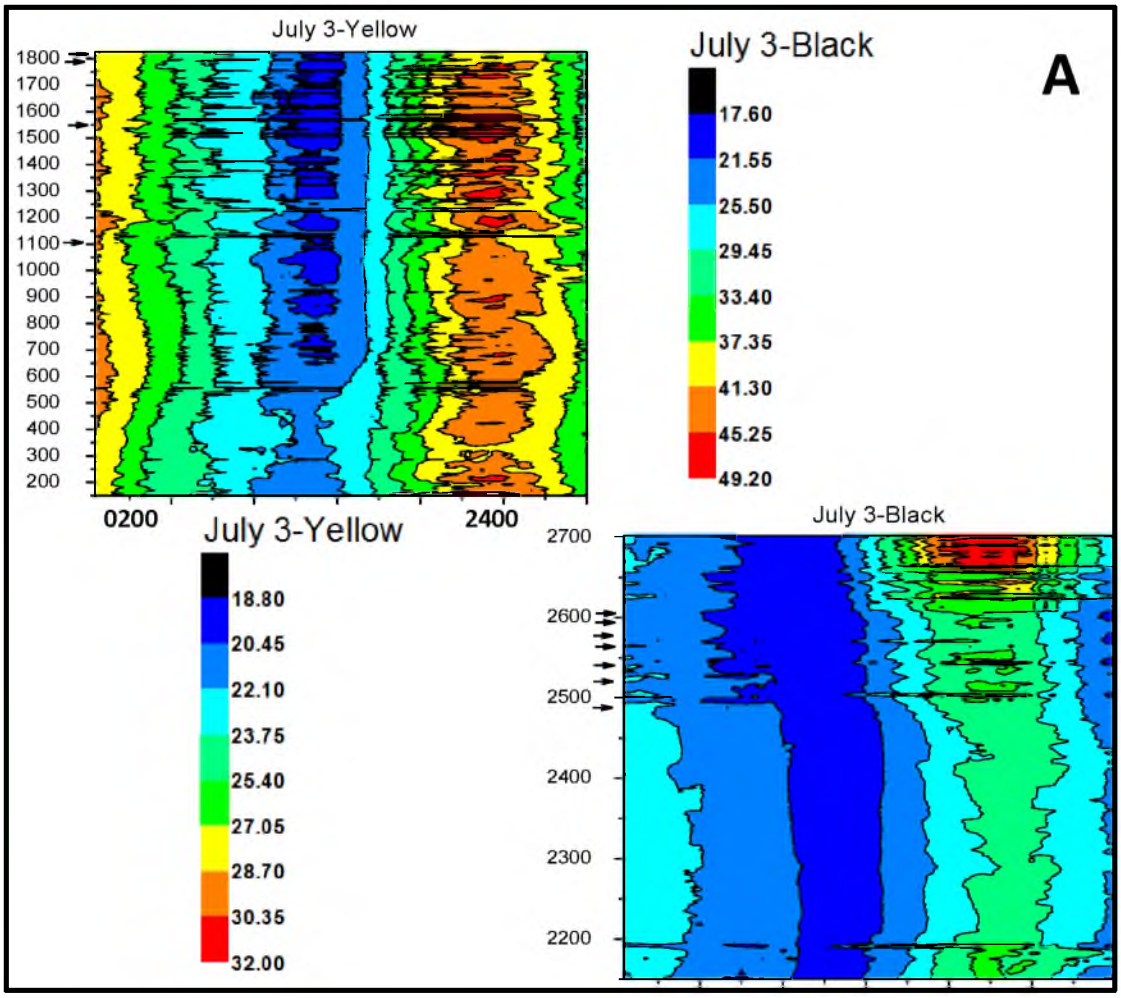

Figure 11: Graphs showing the distributed temperature sensing (DTS) data that were collected during the summer of 2010. These temperature profiles show black arrows where cold temperatures look to persist throughout the day. Each tomogram depicts temperatures in degrees celsius, and the time is MDT (mountain daylight time).

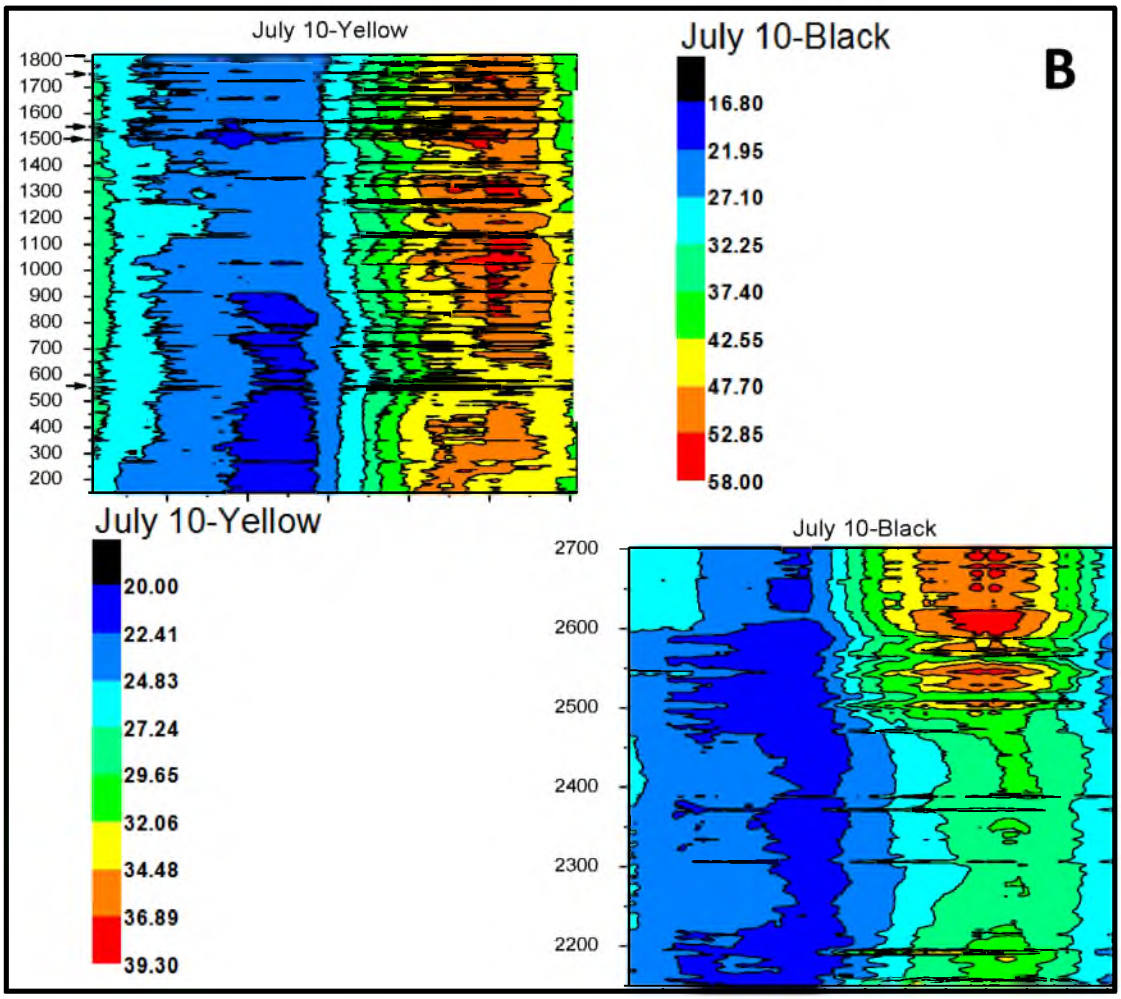

Figure 11 Continued:

conductive layer about 2 m thick with resistivity of about 0.5 ohm-m; (2) a more resistive layer about 3-4 m thick with resistivity about 4 to 5 ohm-m; and (3) a more conductive layer with a resistivity about 0.5 to 1 ohm-m.

The high resistivity anomalies identified by the CRP survey were initially interpreted to indicate areas of less-saline, groundwater or to be a representation of mirabilite in the subsurface. The map of maximum resistivity observed along the boat tracks was compared to cold-water temperature anomalies (Figure 12) to see if the temperature and resistivity anomalies correlate and can be used to show areas for potential groundwater discharge and evidence that the CRP anomalies are less-saline groundwater. Cold-water temperature anomalies appear to be found in the same vicinity as the near-shore high resistivity anomalies. In contrast it appears lower resistivity zones near Saltair marina correspond to areas without cold-water temperature anomalies. However, there are still areas of high resistivity where significant cold-water temperatures are not observed. This suggests that the high resistivity anomalies indicate less-saline groundwater, however groundwater samples from these areas are highly saline (see subsequent sections). Based on these observations, it is likely that the high resistivity zones identified by the near-shore CRP survey indicate the persistent mirabilite layer observed during monitoring well installation.

Comparison of CRP cross sections (Figure 4) with the boring logs, suggests the upper layer includes the water column and sand with hypersaline pore water. The middle layer was first thought to be less-saline groundwater, however after further observation it is interpreted as a mirabilite layer, and the deepest layer is sand with hypersaline pore fluid. Although resistivity decreases with pore-fluid salinity, solid salt layers tend to be

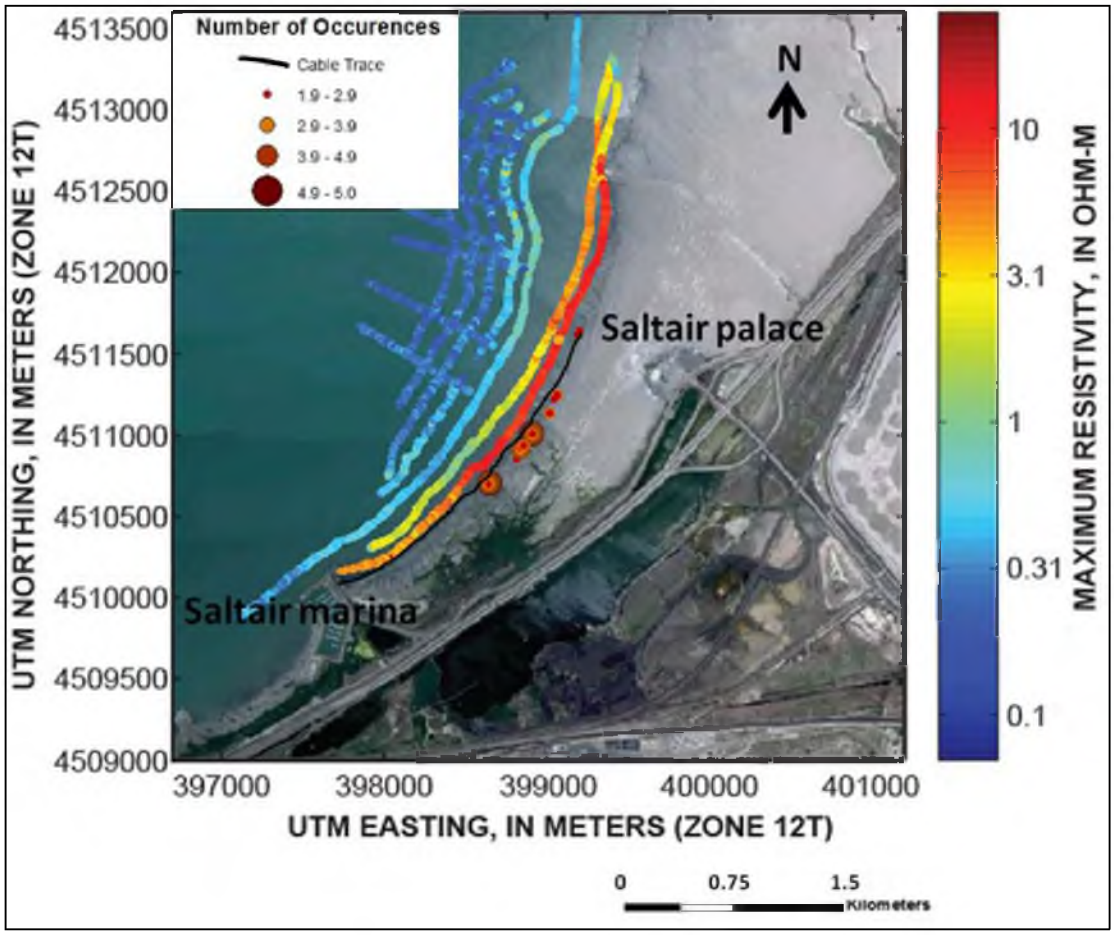

Figure 12: A map showing the maximum resistivity from tomograms, plotted along boat tracks for the Saltair marina area, Great Salt Lake, Utah. Also present are the cold-water temperature anomaly circles which were observed from the fiber-optic distributed temperature survey (FO-DTS).

electrically resistive. For example, solid halite resistivity can be as high as 1013 ohm-m, and solid potassium chloride as high as 1014 ohm-m (Telford et al., 1990).

Further offshore (profiles c, b, and a in Figure 4, depth to the mirabilite layer appears to decrease to 1 m from profile d to c, and then increase again to 1-2 m in profile b. In profile b, the layer itself may become discontinuous in a W-NW direction towards the lake. As seen in the tomogram for profile b, the resistivity anomaly interpreted as the mirabilite layer either becomes more heterogeneous or less resistive overall-possibly indicating development of porosity, solution features, or fractures. In profile a, the resistive layer appears deeper (two to four m below the lake bottom) and yet more heterogeneous and discontinuous. Moving farther offshore, some of the resistivity differences between profiles may result from the different water depth, because sensitivity degrades with increasing water depth. Additional modeling would facilitate interpretation of these data and help confirm the interpretation that the mirabilite layer becomes discontinuous or that its properties change with distance from shore.

Maps based on all resistivity tomograms were prepared to delineate the areal extent of the mirabilite layer and identify zones of possible freshwater discharge. To this end, the highest resistivity seen vertically at every easting-northing for which resistivity estimates are available was plotted (Figure 12). To reduce noise and facilitate visualization of the results, a 5-point zero-phase hanning filter was run horizontally along the calculated maximum resistivity profiles. Maximum resistivity diminishes rapidly with distance from shore. Clear evidence of the mirabilite layer is not apparent in tomograms farther from shore, where CRP sensitivity degrades in deeper and more conductive surface water; however, spatially isolated resistive anomalies are present at

locations along the near-shore tracks.

Seepage meters

Measured seepage rates (Figure 13) determined from seepage meters placed adjacent and north of the fiber-optic cable trace were positive and appear to indicate groundwater discharging in the near-shore areas between the Saltair marina and Saltair palace. The mean seepage rate for the 17 seepage sites was 0.77 cm/day and ranged from 0.01 to 2.37 cm/day. A disadvantage of using the seepage meters is that they only effectively measure flux at a point in space; therefore, for the sake of rough calculations we are assuming these positive seepage rates are consistent over the integrated study area and the average seepage rate is about 0.77 cm/day.

Two of the highest seepage rates (2.37 and 1.34 cm/day) were located near one of the most frequent occurrences of cold-water temperature anomalies; while the lowest seepage rate of 0.01 cm/day is found at the SW end of the fiber-optic cable trace which has fewer than 2 cold-water temperature anomalies. Aside from these three examples, there does not appear to be a strong correlation between the occurrence of cold-water temperature anomalies and the high seepage flow rates found in the near shore regions with water depths of 30-50 cm. For example, a seepage rate of 1.41 cm/day was measured along a portion of the fiber-optic cable trace where no cold-water temperature anomalies were observed.

Unexpectedly high seepage rates (~1 cm/day) were measured north of the fiber-optic cable where water depths were higher (>1m). According to the CRP results the mirabilite layer appears to pinch out in a W-NW direction from the shoreline. Ignoring the three

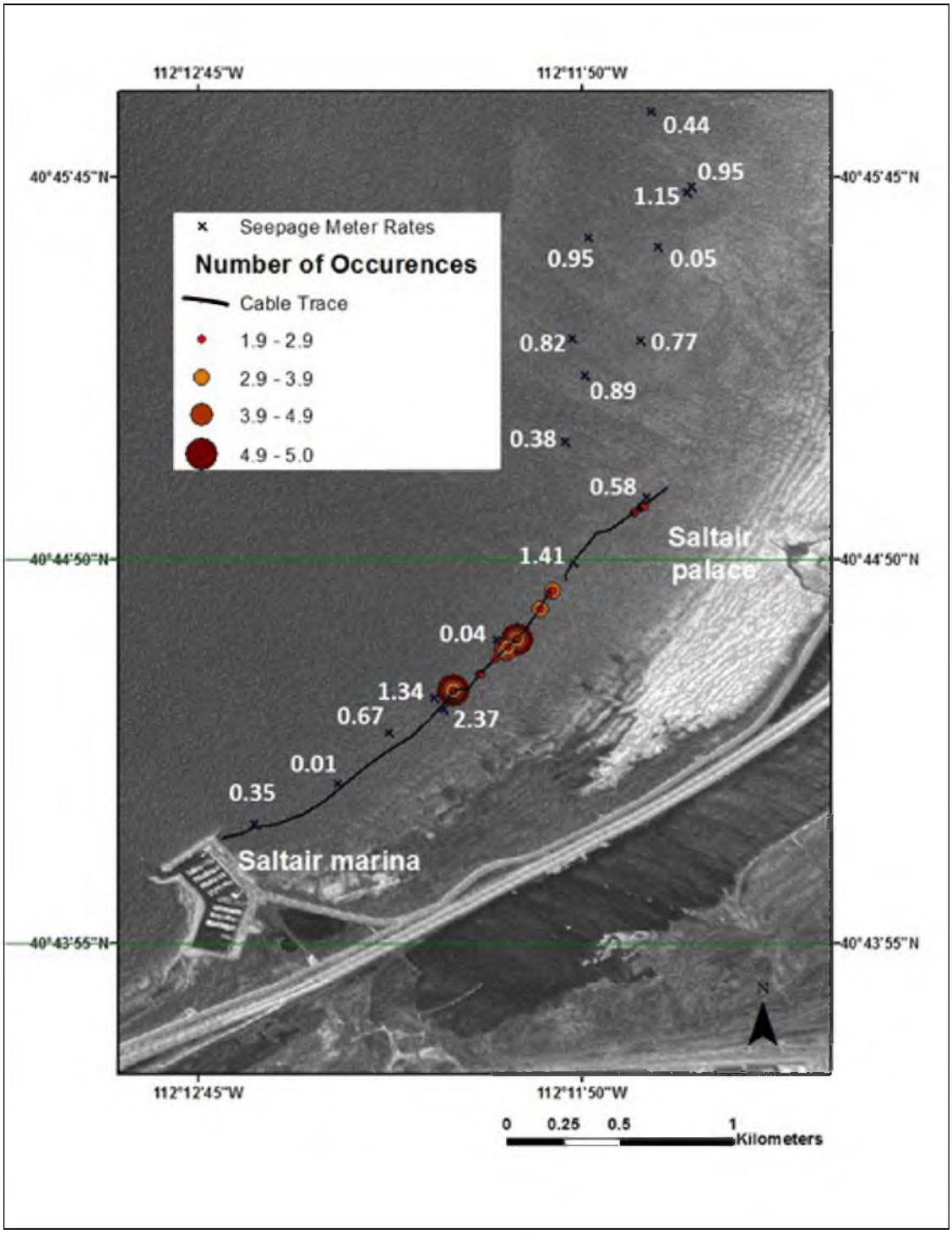

Figure 13: A map of seepage meter locations and their accompanying seepage rates (cm/day) compared with the location of persistent cold-water temperature anomalies found along the fiber-optic cable.

highest and the two lowest seepage rates it appears the seepage rates increase lakeward which could support evidence for the mirabilite pinching out or developing fractures or high porosity.

Water-level monitoring

The first attempt at installing shallow monitoring wells using a diamond core drill bit attached to a gas powered auger was not successful. During the drilling process a hard, salt layer was encountered about 23-38 cm below the sediment-water interface. The hard salt layer was identified as mirabilite ($Na_2SO_4 \cdot 10\ H_2O$) a sodium sulfate deposit that precipitates out of the brines of GSL during the winter time when temperatures are low. It is also described as hard, brittle beds of Glauber's salt that is mixed with sand and clay (Wilson and Wideman, 1957). Glauber's salt was also encountered while the pilings were driven to support the Saltair pavilion (Miller, 1980) which is in the vicinity of the present Saltair palace located within the study area (Figure 1). Each well had a faint H_2S smell permeating from the extracted water that decreased in potency as the water changed from a murky dark gray to clearer water over time. Based on the drill report the mirabilite nearest the shore is ~ 6 m thick and appears to confine the aquifer. According to the CRP results the mirabilite layer pinches out lakeward in a W-NW direction, however this theory is only supported by ignoring the three highest and the two lowest seepage rates. High seepage rates were observed near the shore where the mirabilite is still quite thick, thus suggesting the mirabilite may be impermeable or there is a conduit for groundwater discharge. The other possible hypothesis is the seepage rates are measuring a positive seepage in the top 1 m of sand, above the salt layer which as outlined below, may be

more likely.

To determine if the aquifer below the mirabilite layer is confined or unconfined, the water-levels in well 15 No.3 were corrected for barometric pressure (BP) and compared to water-levels of GSL. A pressure transducer was used to monitor the changes in well water elevation and correlate these fluctuations with changes in GSL elevation (U.S. Geological Survey, 2012c) to determine the degree of aquifer confinement. The BP, which is the weight of the air column on the water-level in the well was removed to better interpret the data and determine the barometric efficiency of the aquifer because the pressure transducer was not vented. This was done by taking BP data from the MesoWest Salt Lake International Airport station (Mesowest, 2012) and subtracting this pressure from the total pressure of the nonvented pressure transducer. The reason for subtracting all of the BP was because the well water during stable pressure events appears to follow the same trend and magnitude of the lake changes, suggesting that the aquifer may be semiconfined. A way to determine this is to find times when large seiche events recorded in GSL elevation and compare these trends to the water-level in the well during periods of stable BP. If the water-level in the well follows the same trend and magnitude of change in lake level during periods of stable BP, the aquifer is unconfined. If the opposite trend is observed then the confining layer has grain to grain contact which is absorbing all of the water column pressure from the lake and there is some degree of confinement to the aquifer of interest.

The change in water-level in a well is caused by the difference in pressure being transmitted directly to the free surface and the pressure being transmitted to groundwater in adjacent buried aquifer sediments through overlying material (Landmeyer, 1996). The

barometric efficiency is the ratio of change in hydraulic head to the change in BP and is used as a correction factor to remove barometric effects on water-levels and can also be used to help determine the degree of confinement within an aquifer to which the well is opened (Gonthier, 2007). The magnitude of water-level change and formation pressure change is a function of the degree of aquifer confinement, the aquifer skeletal matrix, and specific weight of groundwater (Fitts, 2002). If the aquifer is totally unconfined, then the lake level will go up exactly the same amount as the water-level in the well; however this will only occur during stable pressure events where changes in BP cannot influence the water elevation in either the lake or the well.

The BP recorded during deployment of the pressure transducer showed high and low pressure events ranging from 776.2 to 740.4 mm Hg. The water-level recorded in the well correlates inversely with the barometric pressure recorded at the same time (Figure 14A). When the barometric pressure increases over the aquifer, the water-level in the well decreased and vice versa. The pressure transducer data were corrected by subtracting the BP compared with GSL elevation between March and April, 2011 (Figure 14B) to determine if there were any correlations between the two data sets. These comparisons were then used to determine if the aquifer is confined, semiconfined, or unconfined. During the time of the aquifer test there were fluctuations in BP (Figure 15), making it difficult to identify stable BP events which would not influence the water column pressure in either the lake or the well. There were however smaller stable portions of the data which were used to investigate the confinement of the aquifer. A time period between March 28 and April 1, 2011 exhibits relatively stable BP (Figure 15A). During this period of BP stability, variations in GSL water elevation (~23 cm) correlate with

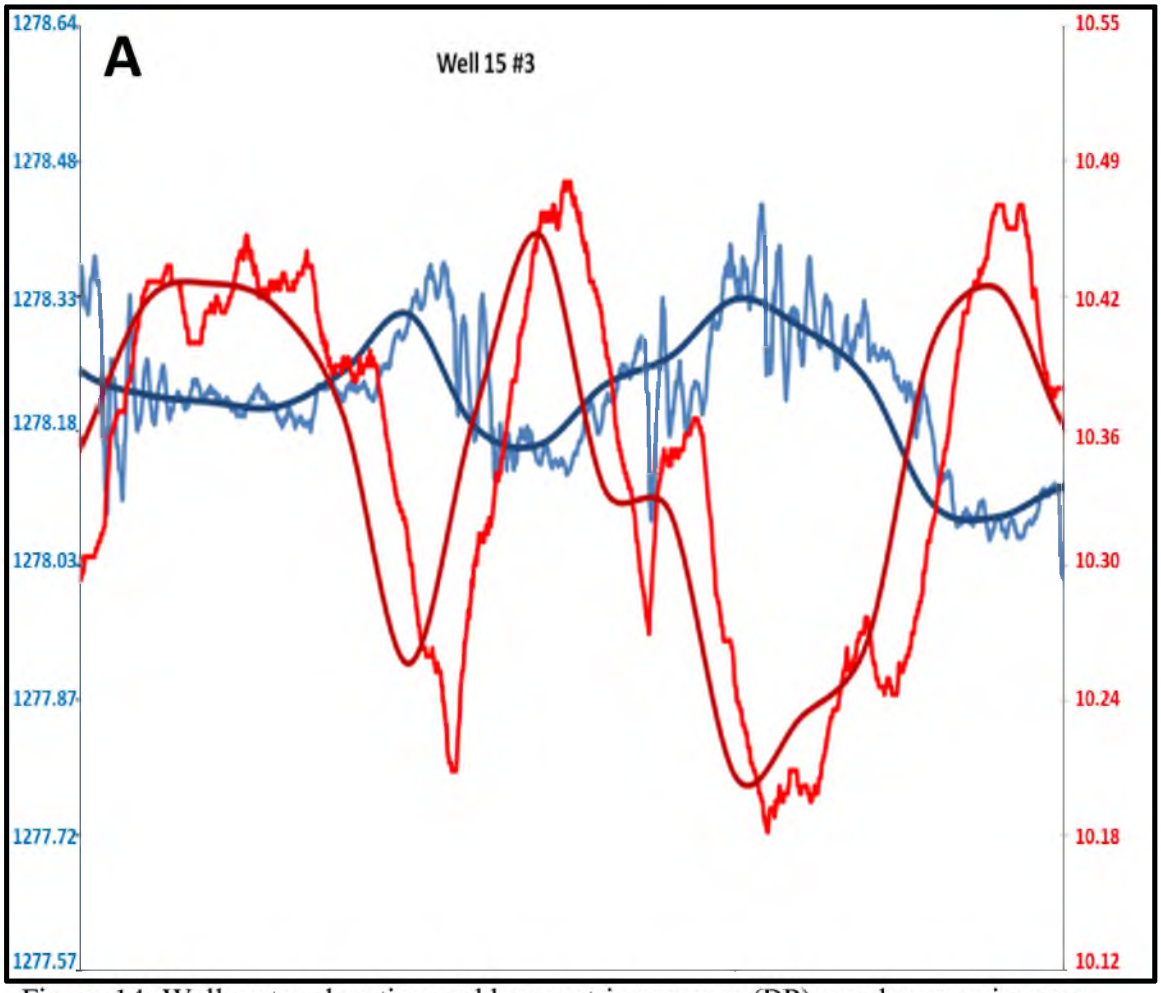

Figure 14: Well water elevation and barometric pressure (BP) are shown as inverse relations to one another. Well water elevation corrected for BP plotted with GSL from March to April 2010.

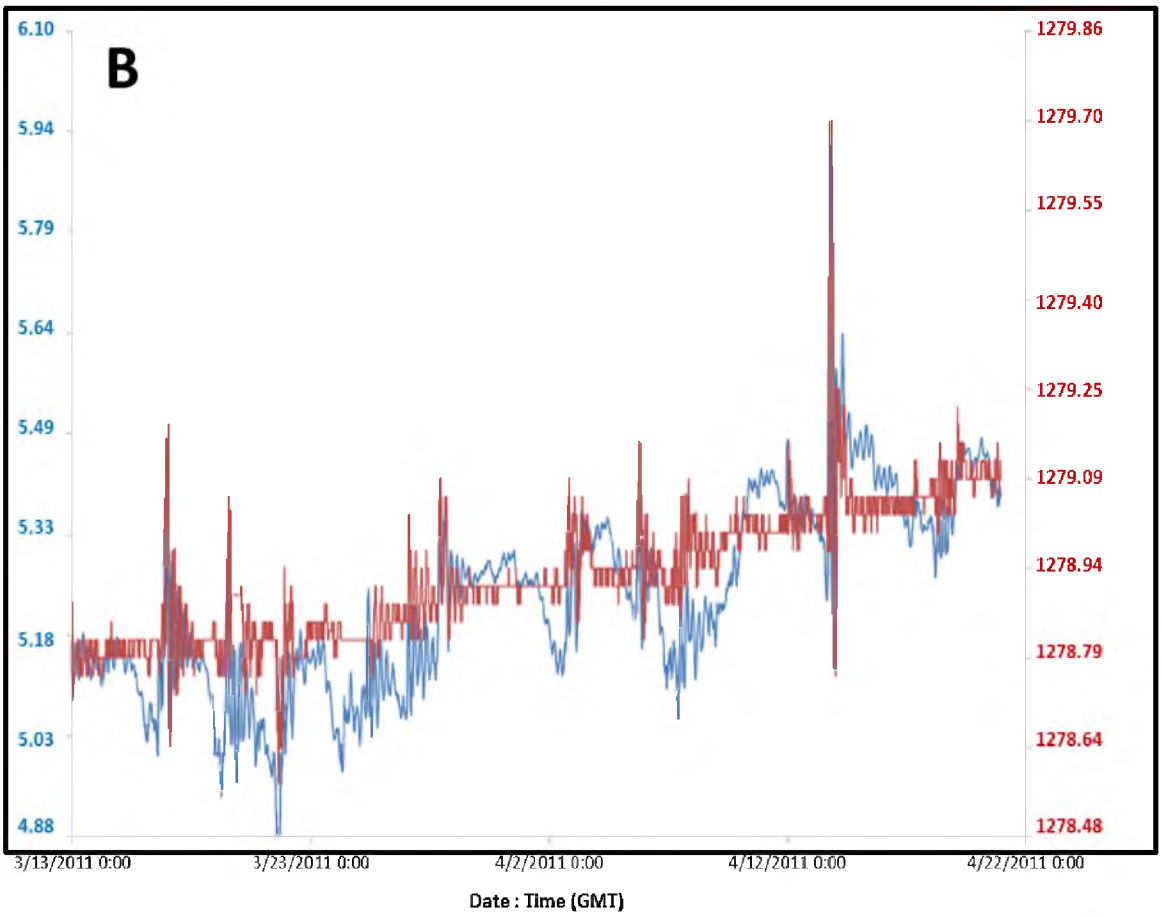
B
6.10
5.94
5.79
5.64
5.49
5.33
5.18
5.03
4.88
1279.86
1279.70
1279.55
1279.40
1279.25
1279.09
1278.94
1278.79
1278.64
1278.48
3/13/2011 0:00
3/23/2011 0:00
4/2/2011 0:00
4/12/2011 0:00
4/22/2011 0:00
Date : Time (GMT)

water level changes in Well 15 No. 3 (~18 cm). The paths are not identical, but do suggest a hydraulic relationship between the aquifer and the overlying GSL. Further evidence of this hydraulic relationship is shown during April 14-15, 2011(Figure 15B), while the change is not as prominent. Further stable pressure events were observed, however during these periods no seiche events could be used for comparison. Based on the 2 seiche events during the monitoring period, the data indicate the aquifer below the mirabilite layer is semiconfined which supports the CRP data showing a thinning or disappearance of the salt layer.

Tritium and dissolved gases

Tritium (^3H) is a radioactive isotope of hydrogen with a half-life of 12.32 years that decays to tritogenic helium-3 ($^3He_{trit}$). Tritium's decay product, $^3He_{trit}$, exists as a noble gas dissolved in water. Concentrations of ^3H are reported as tritium units (TU); one TU is equal to 1 ^3H atom per 10^{18} hydrogen atoms or (3.221 pCi / L) in water. In the earth, small amounts of natural tritium are produced by alpha decay of lithium-7. Natural atmospheric tritium is also generated by secondary neutron cosmic ray bombardment of nitrogen, which then decays to carbon-12 and tritium. Tritium atoms then combine with oxygen, forming water that subsequently falls as precipitation. Since 1954 a large amount of anthropogenic tritium has been injected into the atmosphere as a result of the above ground thermonuclear bomb testing. Since the late 1950s, tritium has rained out of the atmosphere, and can now be used as a tracer in groundwater and help determine its recharge age. Prior to atmospheric nuclear bomb testing in the 1950s, groundwater will have ^3H that has decayed from background "prebomb" concentrations of about 6– 8 TU

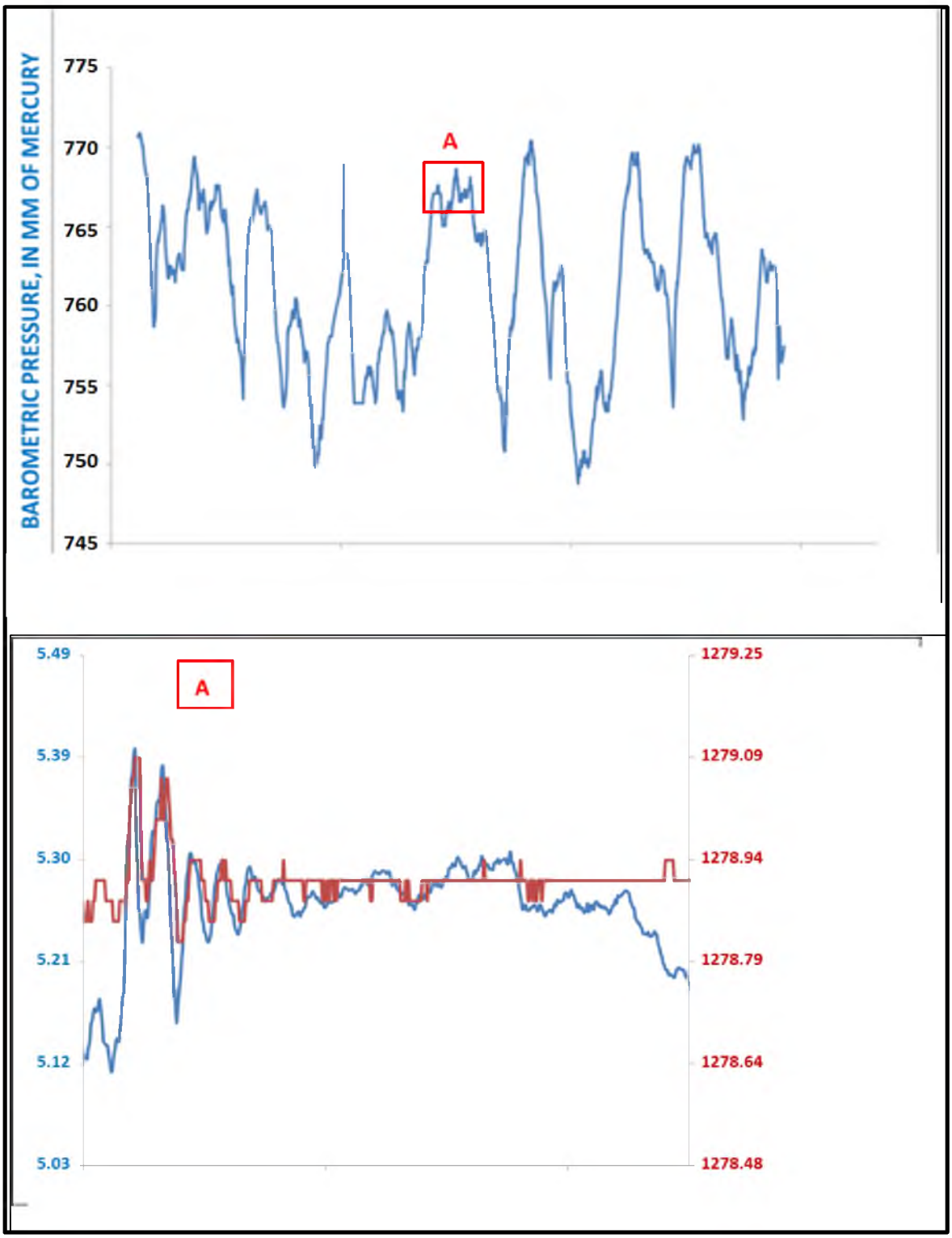

Figure 15**:** Fluctuations in barometric pressure (BP) were recorded in the spring of 2011. The red boxes show areas which depict relatively stable pressure events which are shown in plots A and B. The plots show how the well water follows the trends of the GSL elevations during stable pressure events.

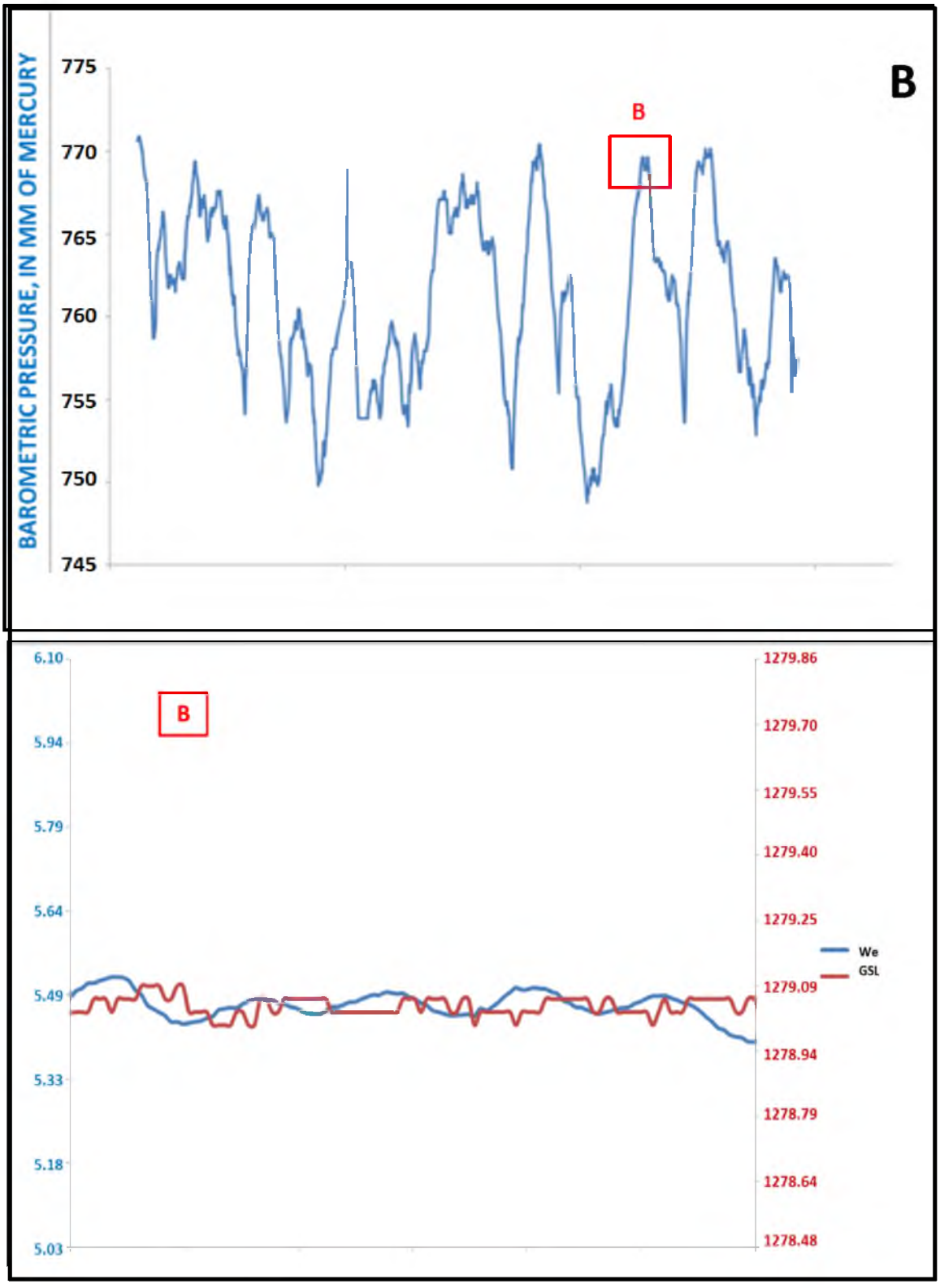

Figure 15 Continued:

to less than 0.3 TU (Schlosser et al., 1988). Because groundwater tritium concentrations reflect atmospheric tritium levels when the water was last in contact with the atmosphere, tritium can be used to semiquantitatively determine whether or not the water is prebomb era (>50 yrs) or postbomb era (<50 yrs).

Water in well 15 No. 3 had 1.1 TU (Table 1), indicating it contains a component of groundwater that was recharged within the last 60 years. The surface water sample collected from the open water of GSL near Well 15 had 6.6 TU, indicating that the water has ^{3}H of modern precipitation. One of the fresh water inflow sites entering the lake (GSL Inflow 2) had 3.9 TU. The open water sample has the ^{3}H concentration of modern precipitation which is likely the result of direct contact with the atmosphere. The water sample from GSL Inflow 2 contained a slightly lower ^{3}H concentration suggesting that it is a mixture of modern surface water diluted with low TU groundwater. The well water sample has >1 TU indicating that it clearly contains at least a small fraction of modern water.

Dissolved noble gases (He, Ne, Ar, Kr, and Xe) provide unique and valuable information in hydrologic studies because of their conservative nature which allows estimation of water table temperatures at the time of groundwater recharge (Manning and Solomon, 2003). It is common for groundwater to contain dissolved gas concentrations greater than equilibrium concentration with respect to atmospheric pressure. The dissolved gas concentrations (Table 1) are all below equilibrium gas solubility, indicative of degassing likely caused by gas stripping (Cey et al., 2009). The groundwater sampled for dissolved gases shows evidence of degassing because the measured total dissolved gas pressure (TDGP) (0.9-1.2 atm) was higher than the expected atmospheric TDGP of

Field ID	Well 11 NO. 1	Well 11 NO. 2	GSL Inflow	Well 01	GSL Inflow 2	Well 15 NO. 1	Well 15 NO. 2	Well 15 NO. 3	Open Water	Well 04
Temperature (^{O}C)	9.0	NA	4.7	10.2	4.4	8.3	7.8	12.9	4.9	9.0
pH	7.1	7.3	8.6	6.7	8.4	6.9	7.8	6.6	8.3	7.0
Dissolved Oxygen (mg/L)	< 0.1	< 0.1	2.6	< 0.1	12.2	< 0.1	< 0.1	< 0.1	7.1	< 0.1
Specific Conductance (µS/cm)	284,000	277,600	8,720	267,500	7,510	277,000	281,000	208,000	193,100	262,100
Sulfide (mg/L)	15	15	NA	30	NA	25	15	30	NA	NA
ORP (mV)	-294	-286	NA	-260	-161	-303	-292	-291	-114	-228
Charge Balance (% difference)	NA	-5.0	NA	-4.5	-3.5	NA	NA	-6.7	-8.8	-4.5
Ca^{2+} (mg/L)	NA	484	116	173	119	NA	NA	202	212	164
Mg^{2+} (mg/L)	NA	6,758	103	8,311	80	NA	NA	6,829	3,101	8,518
Na^{+} (mg/L)	NA	66,060	1,370	103,600	1,148	NA	NA	94,720	29,940	99,010
K^{+} (mg/L)	NA	4,210	57.3	5,077	43.4	NA	NA	4,410	2,113	5,378
Fe (mg/L)	NA	320	8	320	7.1	NA	NA	320	224	320
H^{+} (mg/L)	7.0E-05	5.7E-05	NA	2.1E-04	4.0E-06	NA	NA	2.3E-04	5.0E-06	9.6E-05
Br^{-} (mg/L)	NA	82.3	1.5	87.3	1.3	NA	NA	83.8	39.4	96.4
Cl^{-} (mg/L)	NA	120,154	2,310	172,117	1,984	NA	NA	152,700	62,567	169,491
SO_4^{2-} (mg/L)	NA	25,908	533	46,105	395	NA	NA	56,543	7,810	40,564
Alkalinity as CO_3^{2-}(mg/L)	NA	243	242	502	196	NA	NA	596	322	401
HCO^{3-}(mg/L)	NA	NA	NA	NA	NA	NA	NA	NA	NA	NA
TDS @180^{O}C (mg/L)	NA	198,981	NA	275,749	4,170	NA	NA	263,737	100,187	270,901
Se (ug/L)	NA	0.9	4.8	1.1	5.6	NA	NA	2.3	1.9	1.0
^{3}H (pCi/L)	NA	NA	NA	NA	12.5	NA	NA	3.7	21.1	NA
^{3}H (TU)	NA	NA	NA	NA	3.9	NA	NA	1.1	6.6	NA
O^{18}/O^{16} in SO_4^{2-}(permil)	NA	NA	7.2	13.0	NA	NA	NA	12.9	9.8	NA
S^{34}/S^{32} in SO_4^{2-}(permil)	NA	NA	11.6	19.7	NA	NA	NA	19.9	17.9	NA
$^{2}H/^{1}H$ in H_2O (permil)	-58.8	NA	-107	NA	NA	-57.8	-57.1	NA	NA	NA
O^{18}/O^{16} in H_2O (permil)	-4.55	NA	-13.45	NA	NA	-4.52	-4.39	NA	NA	NA
Copper tube:^{129}Xe (ccSTP/g)	NA	NA	NA	NA	NA	NA	NA	1.4E-09	NA	NA
Diffusion Sampler:^{129}Xe (ccSTP/g)	NA	NA	NA	8.8E-10	NA	NA	NA	9.0E-10	NA	NA
Copper tube:N_2 (ccSTP/g)	NA	NA	NA	NA	NA	NA	NA	3.1E-03	NA	NA
Diffusion Sampler:N_2 (ccSTP/g)	NA	NA	NA	1.9E-03	NA	NA	NA	8.8E-04	NA	NA
Copper tube:^{40}Ar (ccSTP/g)	NA	NA	NA	NA	NA	NA	NA	3.7E-05	NA	NA
Diffusion Sampler:^{40}Ar (ccSTP/g)	NA	NA	NA	3.7E-05	NA	NA	NA	4.8E-05	NA	NA
Copper tube:^{84}Kr (ccSTP/g)	NA	NA	NA	NA	NA	NA	NA	9.9E-09	NA	NA
Diffusion Sampler:^{84}Kr (ccSTP/g)	NA	NA	NA	8.0E-09	NA	NA	NA	8.3E-09	NA	NA
Copper tube:^{20}Ne (ccSTP/g)	NA	NA	NA	NA	NA	NA	NA	2.6E-08	NA	NA
Diffusion Sampler:^{20}Ne (ccSTP/g)	NA	NA	NA	1.6E-08	NA	NA	NA	3.2E-08	NA	NA
Copper tube:^{4}He (ccSTP/g)	NA	NA	NA	NA	NA	NA	NA	4.0E-07	NA	NA
Diffusion Sampler:^{4}He (ccSTP/g)	NA	NA	NA	2.2E-08	NA	NA	NA	2.5E-07	NA	NA
R/R_a	NA	NA	NA	0.44	NA	NA	NA	1.7E-01	NA	NA

0.85 atm, therefore the dissolved gases could not be used to derive recharge temperatures because the data were not reliable. The high TDGPs which suggest degassing in the solution may be influenced by (1) excess air, (2) gas producing reactions in the subsurface, or (3) gas solubility reductions due to the high salinity of the groundwater.

Dissolved helium in groundwater is derived from atmospheric and terrigenic sources. The absolute abundance of helium in systems is difficult to interpret since helium is so mobile and determination of its source is difficult (Solomon and Cook, 2000). Thus, the $^{3}He/^{4}He$ ratio (R) is usually used as a proxy for ^{3}He content; R is generally expressed as a multiple of the present-day atmospheric $^{3}He/^{4}He$ ratio (Ra), which is 0.17-0.44. Calculated R/Ra values in the groundwater samples (Table 1) of < 1 suggest significant amounts of ^{4}He in the groundwater which would indicate old groundwater. Although the ^{4}He is affected by the same degassing (observed in the other dissolved gases; these samples lost an unknown amount of gas leaving only a "minimum" concentration), the ^{4}He is still high enough to indicate the groundwater has an unknown fraction of old water (>1,000 years).

Tritium also decays to ^{3}He by beta particle emission, and knowing this decay rate allows for a more accurate shallow groundwater recharge age. $^{3}H/^{3}He$ ratios are useful for groundwater ages < 50 years. However, because of the degassing issue with our groundwater sample and the data for the ^{4}He concentrations being unreliable this age determination could not be done.

GEOCHEMISTRY RESULTS AND DISCUSSION

Major and minor ions

The charge balance for the 4 shallow groundwater wells and the two fresh water inflow sites are generally within ± 5-7% (Table 1) suggesting the major-ion analyses of these water samples are acceptable. The sample collected near open water of GSL near Well 15 has a charge balance (-8.8) which is not necessarily reason for concern because the high concentration of ions due to the salinity of the water may interfere with eachother during analysis (Watson, 1997). The shallow groundwater is a sodium-chloride water type, and classified as a brine because of the total dissolved solids > 35,000 mg/L (Drever, 1997), and the specific conductance is > 200,000 µS/cm. The brine groundwater has higher concentrations of both sodium and sulfate than the three surface water samples, likely due to mirabilite dissolution.

Bromide and chloride ratios can be used to identify the source of the groundwater because bromide and chloride concentrations up to 20% salinity are considered conservative in nature (Davis et al., 1998). The water samples from the seven shallow groundwater wells, the two fresh water inflow sites, and the one open water of GSL near Well 15 were compared to historic samples collected from the south arm of GSL (unpub. Undergrad research, 2002) (Figure 16). The shallow groundwater samples collected during the study have similar Br:Cl ratios that are distinctly different than surface water samples collected from GSL and the surface water inflow sites within the study area.

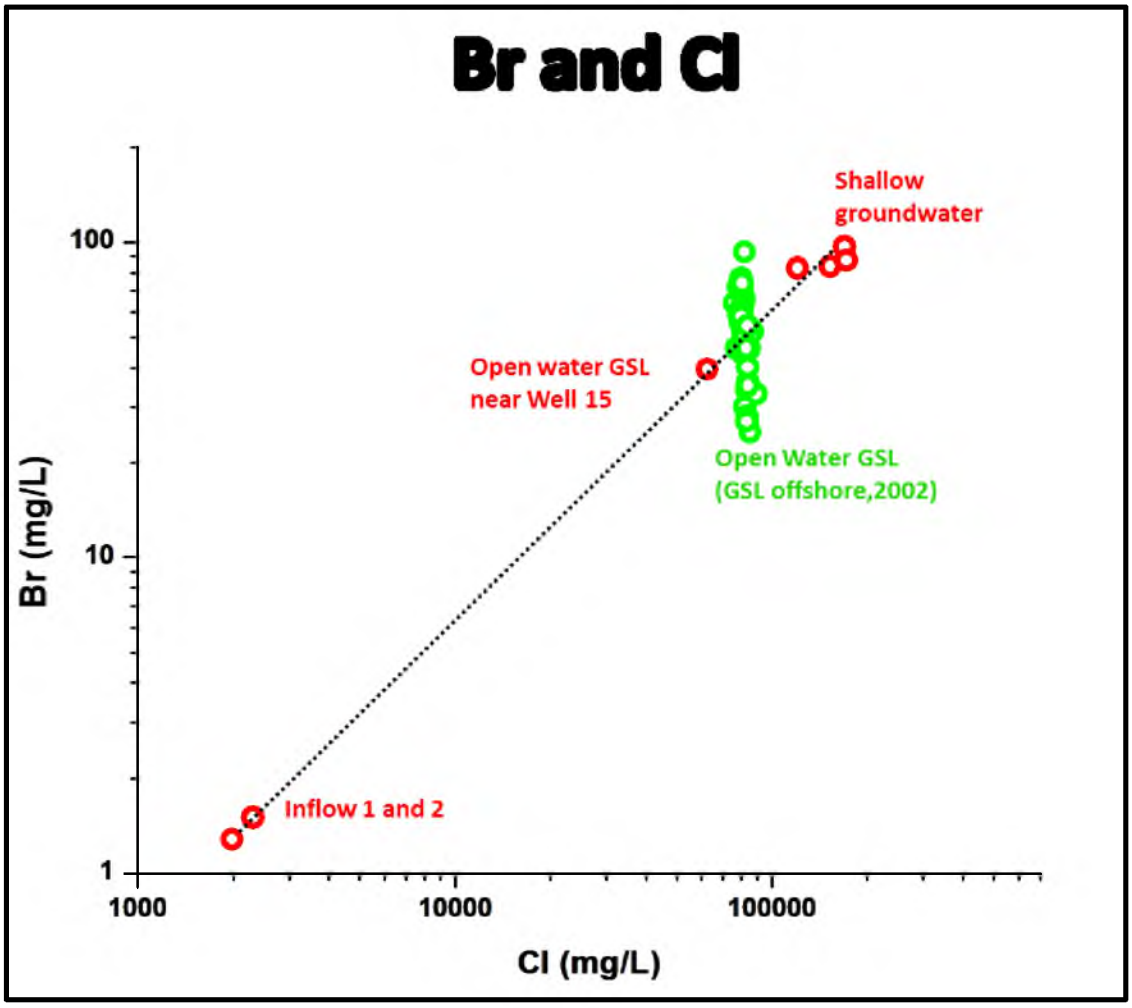

Figure 16: A plot of the bromide vs. chloride concentrations which were collected in different water samples (mg/L). The water samples from the seven shallow groundwater wells (shallow groundwater), the two fresh water inflow sites (inflow 1 and 2), and the open water of GSL near Well 15 were plotted up next to some open water GSL sites taken from the research of Knudson, 2002. Note how the open water GSL near Well 15 does not plot up right next to the other open water GSL samples.

The distinct Br:Cl ratios associated with the shallow groundwater samples indicate limited mixing with surface water from GSL. This distinct Br:Cl ratio of the shallow groundwater suggests the mirabilite salt layer isolates the shallow groundwater from mixing with surface water from GSL. Additional Br:Cl ratio data from the shallow groundwater in areas where the CRP data indicate thinning/disappearance of the salt layer should be collected to determine if mixing with surface water from GSL is indicated in this part of the shallow aquifer. Furthermore, the different Br:Cl ratios between the shallow groundwater and surface water of GSL indicates the origin of the shallow groundwater is different.

Trace elements

Total Hg concentrations in all of the water samples were < 0.005 μg/L. Methyl mercury species were not determined; however the sulfide concentrations measured in the shallow wells (30 mg/L) and the associated anoxic conditions that were observed may be conducive to mercury methylation. Previous work (Naftz et al., 2008) found elevated concentrations of methyl mercury in water samples from the deep brine layer of GSL with similar geochemical conditions.

The dissolved Se concentrations measured near the Saltair marina in 4 shallow groundwater wells, two fresh water inflows to the lake, and one open water of GSL near Well 15 were compared to dissolved selenium data collected from four GSL open water sites and six freshwater inflows entering the South arm of GSL during a 2006-2008 study (Naftz et al., 2008). The Se concentrations (Table 1) in the four shallow groundwater wells, the two freshwater inflow sites, and the open water site near Well 15 were 0.9-2.3

μg/L , 4.8 and 5.6 μg/L, and 1.9 μg/L, respectively. The two fresh water inflows entering the lake had about twice as much Se concentrations relative to all of the inflow sites (~ 2 μg/L) in the 2006-2008 study, except for KUCC inflow (Figure 17A). The open water of GSL near Well 15 had Se concentrations 3 -4 times higher than the four open water sites in the south arm of GSL (~ 0.5 μg/L) in the 2006-2008 study (Figure 17B). The water sample from the open water of GSL near Well 15 was sampled during calm conditions and the elevated Se concentrations likely reflect the influence of inputs from the fresh water inflows and/or the shallow groundwater, both having higher Se concentrations than water samples collected from the open water of GSL during 2006-2008 (Naftz et al., 2008).

The water-level, Br:Cl ratio, and CRP data indicate that the aquifer below the mirabilite salt layer is isolated from surface water; therefore the positive seepage rates measured are likely from the top 1 m of sediment above the salt layer acting as a shallow aquifer which transmits shallow groundwater discharge to GSL. Se concentrations in the top 1 m of sediment were not measured; so it is hard to say how much Se mass input may be contributed through this shallow conduit above the salt layer. As a result, the best estimate of Se mass input may come from surface water inflows by assuming the water is being recharged from higher elevation wetlands above the shoreline of GSL. The following calculation was used to estimate a semiquantitative Se mass input that may be contributed to the south shore of GSL for the duration of one year. Using the average value obtained from the filtered Se concentrations measured in the surface water inflows (5.2 μg/L) and assuming seepage rates of 0.77 cm/day over the entire study area of 1.6 km^2:

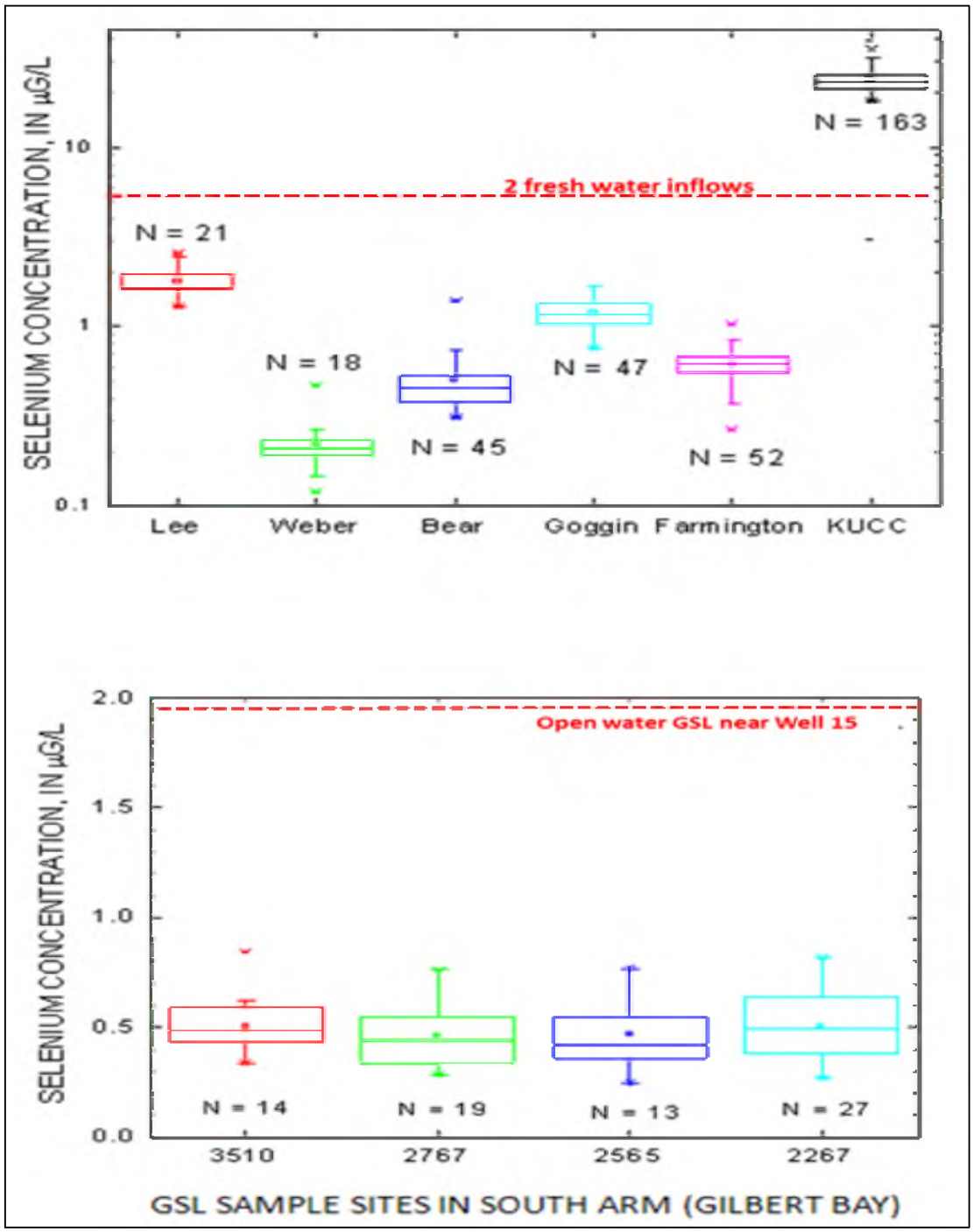

Figure 17: (A). A Box plot that shows the dissolved Se concentrations which were measured in the open water of GSL during a study in 2006 – 2008 from different open water sites. These concentrations are compared to the Se concentration measured from an open water of GSL near Well 15 during the summer of 2010 (B). Note that the Se concentrations from the 2010 study are higher, with the exception of KUCC.

Se mass loading (kg/year) = Area (cm^2) * seepage rate (cm/year) * Se concentration (kg/L)

Se mass loading = (1.6E +10 cm^2) * (282 cm/year) * (5.2E -9 kg/L) * (0.001 L/cm^3)

Se mass loading = 23.5 kg/year

The Se mass loading from surface water discharge is quite small; < 2 % of the missing Se which could exceed 1500 kg/year (Naftz et al., 2008). It would appear based on the above estimates that Kennecott's initial modeling results suggesting elevated Se concentrations in groundwater beneath the KUCC refinery contributes minimal discharge to GSL is confirmed, however this does not account for Se concentrations which may be in the top 1 m of sediment above the salt layer.

Stable isotopes

Deuterium and oxygen-18 (δD and $\delta^{18}O$) isotopic values measured near the Saltair marina in seven shallow groundwater wells, two fresh water inflows to the lake, and one open water of GSL near Well 15 were compared to δD and $\delta^{18}O$ isotopic data collected from groundwater near Toole Valley, Utah (Stolp and Brooks, 2009) as well as surface water samples from the south arm of GSL (Knudson, 2002) (Figure 18A). With the exception of the groundwater samples from the Tooele Valley basin all of the water samples plot below the global meteoric water line (Craig, 1961), which is a possible indication of evaporation (Drever, 1997). A hypothetical mixing line was constructed between the isotopically light groundwater samples collected near Toole, Utah (Stolp and Brooks, 2009) with the most isotopically enriched surface water samples from the south arm of GSL (Knudson, 2002) (Figure 18A). Consistent with the Br:Cl ratio results, the δD and $\delta^{18}O$ values of the water samples from the shallow groundwater are isotopically

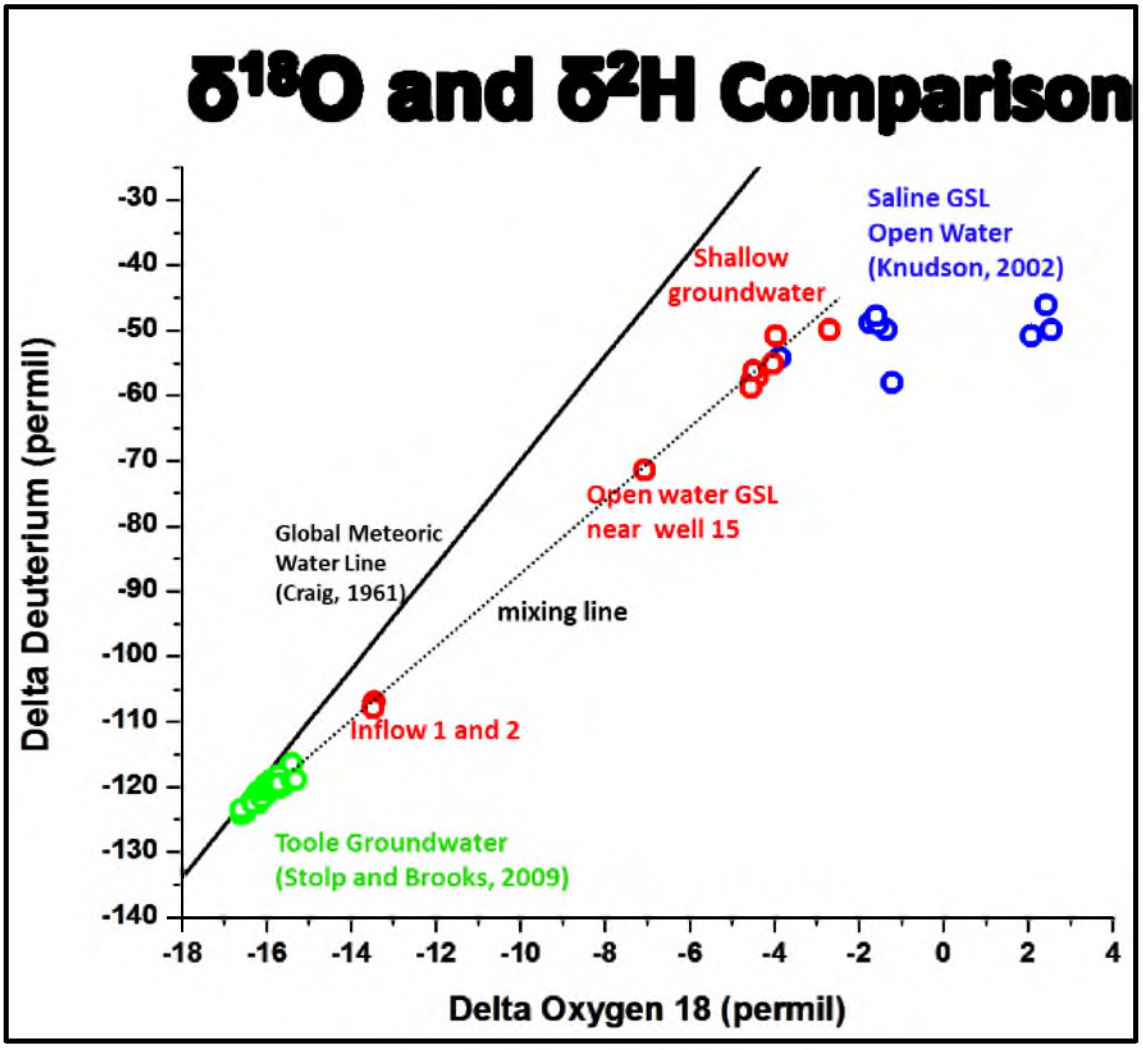
δ18O and δ2H Comparison
Delta Deuterium (permil)
-30
-40
-50
-60
-70
-80
-90
-100
-110
-120
-130
-140
-18
-16
-14
-12
-10
-8
-6
-4
-2
0
2
4
Delta Oxygen 18 (permil)
Saline GSL
Open Water
(Knudson, 2002)
Shallow
groundwater
Open water GSL
near well 15
Global Meteoric
Water Line
(Craig, 1961)
mixing line
Inflow 1 and 2
Toole Groundwater
(Stolp and Brooks, 2009)

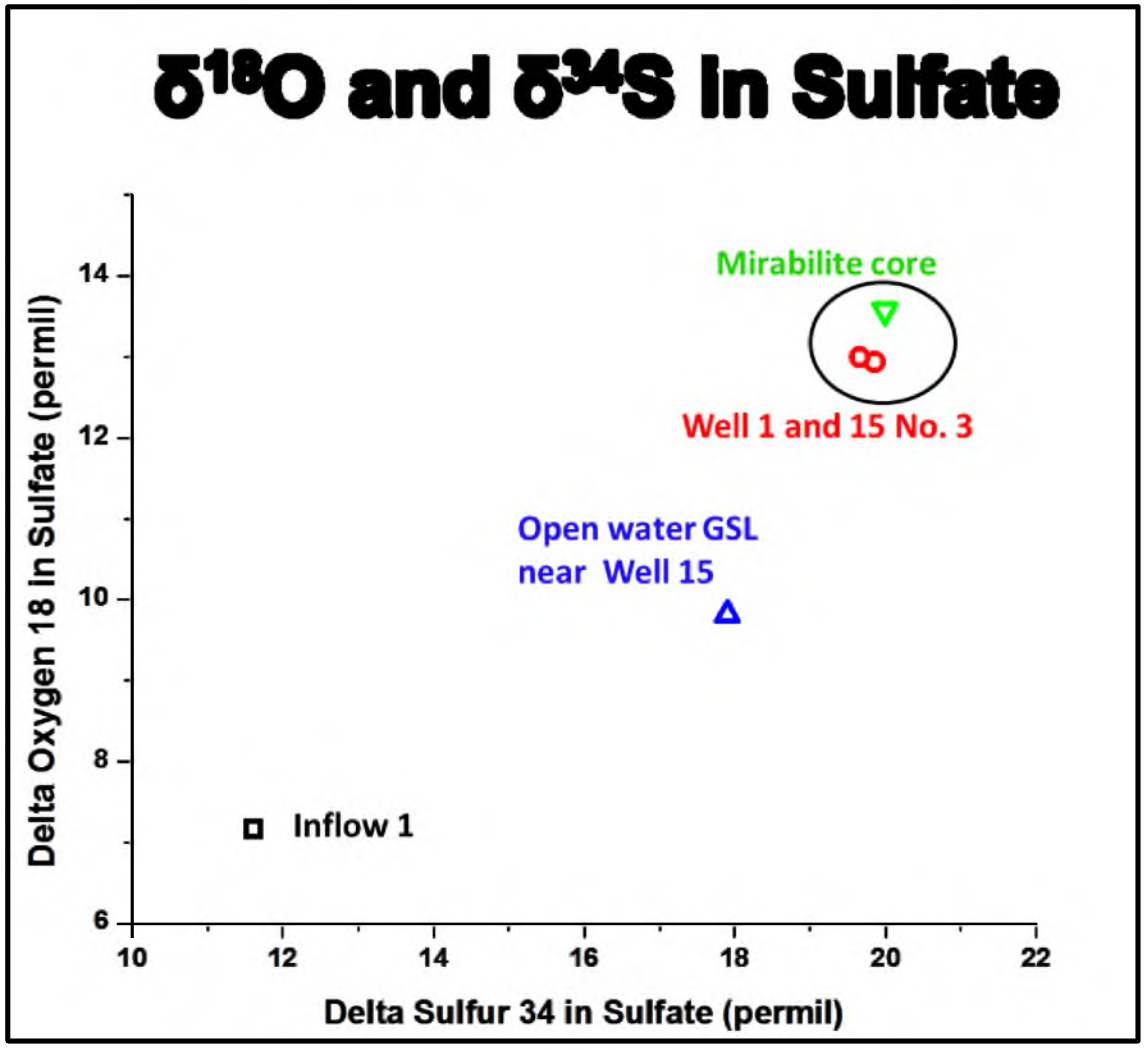
δ18O and δ34S in Sulfate
Mirabilite core
Well 1 and 15 No. 3
Open water GSL
near Well 15
Inflow 1
Delta Oxygen 18 In Sulfate (permil)
Delta Sulfur 34 in Sulfate (permil)
14
12
10
8
6
10
12
14
16
18
20
22

lighter than water samples from the south arm of GSL. This difference could be due to different water sources or possibly due to changes in the δD and $\delta^{18}O$ values in the south arm of GSL over time.

The isotopically enriched values of inflows 1 and 2 relative to the groundwater samples collected near Toole suggest that this water has undergone evaporation or mixing with an isotopically enriched water. The wetland areas southeast of the GSL shoreline could represent an area where evaporation could take place prior to discharge of these seeps to GSL. Large seiche events in the study area could be a transient source of isotopically enriched water from GSL to the shallow sediments overlying the salt layer.

The lighter δD and $\delta^{18}O$ values observed in the near-shore water sample from GSL (collected near Well 15) likely reflects significant mixing with the shallow surface seeps discharging in this part of the study area. This mixing process is also consistent with the elevated Se concentrations and the Br:Cl ratios detected in the near-shore water sample collected from the open water of GSL. Based on the mixing line proportions, the isotopic values of the open water of GSL near Well 15 may be composed of ~40% of water from the 2 fresh water inflows entering the lake.

Filtered water samples collected from Inflow 1, open water of GSL near Well 15, and shallow groundwater from Wells 1 and 15 No. 3 were analyzed for $\delta^{34}S_{sulfate}$ and $\delta^{18}O_{sulfate}$. The resulting isotopic values were compared to the $\delta^{34}S_{sulfate}$ and $\delta^{18}O_{sulfate}$ values determined from a solid-phase sample of the salt layer removed during the drilling of the monitoring wells (Figure 18B). The similar isotopic signatures between the mirabilite core sample to the isotopic signature of the 2 shallow groundwater samples (Well 15 No.3 and Well 1) indicate that the shallow groundwater is significantly

influenced by the dissolution of the mirabilite that is in contact with. Furthermore, the $\delta^{34}S_{sulfate}$ and $\delta^{18}O_{sulfate}$ values in water samples collected from Inflow 1 and the open water of GSL near Well 15 do not indicate significant amounts of mirabilite dissolution (Figure 18B). This is further evidence of the confined/semiconfined nature of the shallow groundwater below the south arm of GSL and its isolation from surface water as indicated by the hydrological and geochemical data.

Geochemical modeling

The stable isotopes and the major ions indicate that the shallow groundwater beneath the salt layer may be obtaining its high sulfate and sodium concentrations from the dissolution of mirabilite. The geochemical model PHREEQC was used to further investigate the effect of mirabilite dissolution on the shallow groundwater geochemistry. The mirabilite SI values were calculated for water samples collected near the Saltair marina in 4 shallow groundwater wells and 1 open-water of GSL near Well 15. The mirabilite SI values for Well 1, Well 4, Well 11 No.2 , and Well 15 No. 3 were 0.03, 0.04, -0.08, 0.06. They were all slightly greater than 0 which indicates the water is at equilibrium with respect to mirabilite (Merkel et al., 2005).

Arsenic concentrations were not determined in the shallow groundwater samples collected during the study; however, a well located 2 km north of the KUCC tailings pond (Figure 1) was sampled by the USGS in August 2011. This groundwater sample contained an As concentration of 200 ug/L, which is elevated relative to As concentrations measured in groundwater from the same area during 1990-1991 (1.5-30 ug/L with a mean concentration of 12.5 ug/L (n=6)). Arsenic concentrations measured in

KUCC tailings pond water collected and analyzed by the USGS from 1972-1984 (Well 404704112060401) ranged from 11-1,900 ug/L with a mean concentration of 220 ug/L (n=27). Selenium concentrations in KUCC tailings pond water measured during 2006-2008 averaged 24 ug/L (n=163) (Naftz et al., 2008); however, Well 404704112060401 contained a Se concentration < 2 ug/L. The PHREEQC geochemical model was used to determine if the likely low redox conditions in Well 404704112060401 would support elevated As concentrations and relatively low Se concentrations (Hockin and Gadd, 2003, Schreiber et al., 2003, Keimowitz et al., 2003). The PHREEQC-Pitzer database was used to model the hypersaline groundwater collected under the hard salt layer, and the Minteq database which is more applicable to freshwater analysis could be utilized to investigate the speciation of As and Se in Well 404704112060401 because the water is relatively fresh. The resulting data (Table 2) suggest under reducing conditions indicative of the low dissolved oxygen values, As-bearing minerals are mobilized (dissolved) while Se-bearing minerals precipitate from the solution. This may explain why the shallow groundwater collected below the salt layer has low concentrations of Se. However, we did not measure As concentrations in the water samples we collected therefore future work should investigate this hypothesis by sampling for As.

Table 2: Selected output of water chemistry for Well 404704112060401 using PHREEQC geochemical modeling.

```
Initial solution 1.  Well 404704112060401
-----------------------------Description of solution----------------------------
                                    pH  =   7.600
                                    pe  =  -1.700
                      Activity of water  =   0.997
                         Ionic strength  =  9.404e-002
                        Mass of water (kg)  =  1.000e+000
                     Total carbon (mol/kg)  =  4.954e-003
                        Total CO2 (mol/kg)  =  4.954e-003
                      Temperature (deg C)  =  15.700
                   Electrical balance (eq)  = -7.608e-003
 Percent error, 100*(Cat-|An|)/(Cat+|An|)  =  -4.26
                               Iterations  =  12
                                  Total H  = 1.110184e+002
                                  Total O  = 5.553264e+001
----------------------------Distribution of species-----------------------------
                                                 Log       Log         Log
   Species                Molality    Activity  Molality  Activity     Gamma
As(3)           2.630e-006
As(5)           5.401e-008

Se(-2)          2.125e-009
Se(4)           7.930e-012
Se(6)           3.153e-011
------------------------------Saturation indices--------------------------------
      Phase               SI log IAP  log KT
      Arsenolite      -19.17  -22.31   -3.14  As4O6
      As2O5           -34.69  -27.86    6.83  As2O5
      Ca3(AsO4)2:6H2O -14.85    7.45   22.30  Ca3(AsO4)2:6H2O
      FeAsO4:2H2O     -11.93  -11.53    0.40  FeAsO4:2H2O
      MgSeO3:6H2O     -10.18   -6.18    4.00  MgSeO3:6H2O
      Mn3(AsO4)2:8H2O -13.60   -1.10   12.50  Mn3(AsO4)2:8H2O

      Ferroselite       7.69  -11.17  -18.86  FeSe2
      FeSe              0.56   -6.60   -7.16  FeSe
      Se(A)             2.60   -4.58   -7.17  Se
      Se(hex)           3.21   -4.58   -7.79  Se
------------------
End of simulation.
```

SUMMARY

Geophysical tools were used to locate potential areas for groundwater discharge and seepage measurements were made to quantify the amount of discharge. Dissolved gas concentrations, environmental isotopes, and water-quality data were collected to better understand how groundwater discharge may be impacting Se concentrations along the south arm of GSL near the Saltair marina. A FO-DTS survey was conducted by arranging 3 km of fiber-optic cable parallel to the lake shore and temperature data were collected every 20 minutes at approximately 1 m intervals from June 11 to July 13, 2010. These temperature data sets were used to generate temperature contour maps which were used to locate areas of groundwater discharge. The cold-water temperature anomalies observed in the temperature tomograms and fiber-optic cable traces were used as guides to place the seepage meters to measure groundwater discharge in the near shore of the Saltair beach. Seventeen standard half-barrel seepage meters were installed in the near-shore of the south arm of GSL near the Saltair marina during the week of July 8-15, 2010. The seepage meters measured positive seepage flux and the mean seepage rate for the 17 seepage sites was 0.77 cm/day, suggesting groundwater discharge to GSL albeit small is occurring near the Saltair marina. There does not appear to be a strong correlation between cold-water temperature anomalies observed in the FO-DTS and the high seepage flow rates.

CRP data were collected along 14 tracks near the Saltair marina to distinguish fresh

from saline groundwater in shallow sedimentary units and distinguish changes in the lithology. The CRP survey indicates there is a hard, impermeable salt layer in the near shore of GSL near the Saltair marina. The hard salt has been identified as mirabilite ($Na_2SO_4 \cdot 10\ H_2O$), and the CRP data suggest this layer is about 6 m thick and appears to pinch out in a W-NW direction towards the lake. An aquifer test was performed by using a pressure transducer to monitor the changes in well-water and to compare these fluctuations to the changes in GSL water elevation and use these correlations to determine the confinement of the aquifer. The pressure transducer data indicates the aquifer below the mirabilite is semiconfined which supports the CRP data showing a thinning or disappearance of the salt layer. There was positive seepage measured in the near shore of GSL near the Saltair marina suggesting the mirabilite may not be as impermeable as it seems or the top 1 m of the sand above the hard salt layer is acting as a shallow aquifer which transmits shallow groundwater discharge. The isolation of the shallow groundwater from mixing with the surface water of GSL is confirmed in the distinct Br:Cl ratios (Figure 16). It would appear based on the CRP, water-level, and Br:Cl ratio data that the aquifer below the mirabilite is isolated from surface water and it is more likely groundwater discharge is coming from the top 1 m of the sand above the salt layer.

The high ^4He concentrations measured in the dissolved gases and the tritium concentrations found in the groundwater suggest this water has components of both old and young groundwater and is likely mixing because regional and local flow paths are converging and discharging into GSL. The Se concentrations collected in the surface water samples during the 2010 study showed elevated concentrations (two to four times

higher) in comparison to Se concentrations from a USGS 2006-2008 study, suggesting there is a Se influence in the area. There are fresh water inflows which are likely groundwater seeps that appear to be mixing with the open water of GSL; evidence for this mixing is found in the δD and $\delta^{18}O$ isotopic values, Br:Cl ratios, and the Se concentrations.

Evidence for the dissolution of mirabilite in the groundwater is found in the isotopic and geochemical data from the shallow groundwater well samples. The $\delta^{34}S$ and $\delta^{18}O$ isotopic signature in the sulfate molecule in the well water is almost identical to the isotopic signature in the mirabilite core material. These data suggest the groundwater obtains its high sulfate concentrations from the dissolution of the mirabilite material, supporting the evidence from the major ions. Also, the hypersaline groundwater has higher concentrations of both sodium and sulfate than the three surface water samples, likely due to mirabilite dissolution as well. Geochemical modeling shows that mirabilite SI values for the shallow groundwater samples were all slightly greater than 0 indicating the water is at equilibrium with respect to mirabilite

The geochemical modeling results suggest that under reducing conditions, As bearing minerals are mobilized while Se bearing minerals precipitate out of solution possibly explaining why the shallow groundwater below the hard salt layer has low concentrations of Se. However, we did not measure As concentrations in the water samples. Therefore it is suggested that future sampling investigate this hypothesis by sampling for As.

If we assume that groundwater discharge is coming from the top 1 m of the sand above the salt layer, then we can do some calculations to determine how much shallow

groundwater may be discharging in the near-shore of the south arm of GSL near the Saltair Marina. However, Se concentrations were not measured in the top 1 m of the sand above the salt layer; so it is difficult to say how much Se mass input may be contributed through this shallow conduit above the salt layer. As a result, the best estimate of Se mass input may come from surface water inflows by assuming the water is being recharged from higher elevation wetlands above the shoreline of GSL. The Se mass loading from surface water discharge is quite small; < 2 % of the reported missing Se. It would appear that Kennecott's initial modeling results suggesting that elevated Se concentrations in groundwater beneath the KUCC refinery contributes minimal discharge to GSL is confirmed, however our calculations do not account for Se concentrations which may be in the top 1 m of sediment above the salt layer.

REFERENCES

Aldrich, T. W. and D. S. Paul. 2002, Avian Ecology of Great Salt Lake. in Gwynn, J. W. Great Salt Lake: an overview of change.Special Publication of the Utah Department of Natural Resources. Salt Lake City, USA. 343–374 p.

Anderson, P.B., and D.D. Susong. 1995, Hydrogeology of recharge areas of the principal aquifers along the Wasatch Front and adjacent areas, Utah, in Lund, W.R., editor, Environmental and engineering geology of the Wasatch Front region: Utah Geological Association Publication 24.249-268 p.

Arnow, T, and J.C. Stephens. 1975, Groundwater inflow to Great Salt Lake, Utah: Geological Society of America Abstracts with Programs, 1975 annual meeting, 81 p.

Belovsky, G. E., D. Stephens, C. Perschon, P. Birdsey, D. Paul, D. Naftz, R. Baskin, C. Larson, C. Mellison, J. Luft, R. Mosley, H. Mahon, J. Van Leeuwen, and D. V. Allen. 2011, The Great Salt Lake Ecosystem (Utah, USA): long term data and a structural equation approach. Ecosphere 2(3):art33. doi:10.1890/ES10-00091.1.

Bengtson , D. A., P. Léger and P. Sorgeloos. 1991, Use of Artemia as a food source for aquaculture. In R. A. Browne, P. Sorgeloos & C. N. A. Trotman. Artemia Biology. Boca Raton, Florida: CRC Press. ISBN 978-0-8493-6729-8. 122–123 p.

Boyle, D.R. 1994, Design of a seepage meter for measuring groundwater fluxes in the nonlittoral zones of lakes-Evaluation in a boreal forest lake. Limnological. Oceanography., 39(3), 1994, 670-681 p.

Brix, K.V., D. K. DeForest, R. D. Cardwell, and W. J. Adams. 2004, Derivation of a Chronic Site-specific Water Quality Standard for Selenium in the Great Salt Lake, Utah, USA. Environmental Toxicology and Chemistry 23(3), March: 606–612 p.

Caudell, J. and M. Conover. 2006, Energy content and digestibility of brine shrimp (Artemia franciscana) and other prey items of eared grebes (Podiceps nigricollis) on the Great Salt Lake, Utah. Biological Conservation 130: 251–254 p.

Cey, B., G. Hudson, J. Moran, and B. Scanlon. 2009, Evaluation of Noble Gas Recharge Temperatures in a Shallow Unconfined Aquifer. Ground Water 47: 646-659 p.

Cherkauer D.S. and J.M. McBride. 1998, A remotely operated seepage meter for use in large lakes and rivers. Ground Water 26:165-171 p.

Craig, H. 1961, Isotopic variations in meteoric waters: Science, v. 133, no. 3465,1702-1703 p.

Cross, V.A., J.F. Bratton, E. Bergeron, J.K. Meunier, J. Crusius, and D. Koopmans. 2006, Continuous resistivity profiling data from the Upper Neuse River Estuary, North Carolina, 2004-2005: U.S. Geological Survey Open-File Report 2005-1306, accessed at http://pubs.usgs.gov/of/2005/1306/.

Cross, V.A., J.F. Bratton, J. Crusius, J.A. Colman, and T.D. McCobb. 2008, Submarine hydrogeological data from Cape Cod National Seashore: U.S. Geological Survey Open-File Report 2006-1169, accessed at http://pubs.usgs.gov/of/2006/1169/.

Davis, S.N., Whittemore, D.O., and Fabryka-Martin, J. 1998, Uses of chloride/bromide ratios in studies of potable water, Ground Water 36(2), 338-351 p.

Day-Lewis, F.D., E.A. White, C.D. Johnson., J.W. Lane J.W, Jr., and M. Belaval. 2006, Continuous resistivity profiling to delineate submarine groundwater discharge-examples and limitations, The Leading Edge,25(6),724–728 p.

Dobrin, M. B. 1976, Introduction to Geophysical Prospecting: McGraw - Hill Book C o., 630 p. Conover, Michael R. "Energy Budgets for Eared Grebes on the Great Salt Lake and Implications for Harvest of Brine Shrimp." Journal of Wildlife Management 73.7 (2009):1134-1139.1 p.

Drever, James I. 1997, Stable Isotopes. In The Geochemistry of Natural Waters: Surface and Groundwater Environments, Prentice Hall, Inc. Upper Saddle River, New Jersey.

Fishman, M.J., and L.C. Friedman. 1989, Methods for determination of inorganic substances in water and fluvial sediments: U.S. Geological Survey Techniques of Water-Resources Investigations, book 5,chap. A1, 545 p.

Fishman, M.J. 1993, Methods of analysis by the U.S. Geological Survey National Water Quality Laboratory--Determination of inorganic and organic constituents in water and fluvial sediments: U.S.Geological Survey Open-File Report 93-125, 217 p.

Fitts, C.R. 2002 Groundwater Science. 2002, Amsterdam; Boston:Academic Press. ISBN No. 0122578554. 127 p.

Gaddis, B. and H. Hornbeck. 2011, Environemental assessment for the Jordan Valley Water Conservancy District Groundwater ectraction and treatment remedial project in the southwest Jordan valley. SWCA Environmental Consultants. Final Report. March 2011. 20 p.

Garbarino, J.R., and D.L. Damrau. 2001, Methods of analysis by the U.S. Geological Survey National Water Quality Laboratory---Determination of organic plus inorganic mercury in filtered and unfiltered natural water with cold vapor--atomic fluorescence spectrometry: U.S. Geological Survey Water- Resources Investigations Report 01-4132, 16 p.

Gardner, P., and D. K. Solomon. 2009, An advanced passive diffusion sampler for the determination of dissolved gas concentrations, Water Resources Research., 45,W06423, doi:10.1029/2008WR007399. 8-9 p.

Gonthier, G.J. 2007, A graphical method for estimation of barometric efficiency from continuous data–concepts and application to a site in the Piedmont, Air Force Plant 6, Marietta, Georgia: U.S. Geological Survey, Scientific Investigation Report 2007–5111, 1 p.

Henderson, R., F. Day-Lewis, , J.,Lane, C. Harvey, and L. Liu. 2008, Characterizing submarine ground-water discharge using fiber-optic distributed temperature sensing and marine electrical resistivity , in Symposium on the Application of Geophysics to Engineering and Environmental Problems, April 6-10, 2008, Philadelphia, Pennsylvania, Proceedings: Denver, Colorado, Environmental and Engineering Geophysical Society, 11p.

Herbert, L.R., R.W. Cruff, and K.M. Waddell. 1985, Seepage study of six canals in Salt Lake County, Utah, 1982-83: Utah Department of Natural Resources Technical Publication No. 82, 95 p.

Hersir, G.P. and Á. Knútur. 2010, Resistivity of rocks. Presented at Short Course Von Exploration for Geothermal Resources, organized by UNU-GTP, GDC and KenGen, at Lake Bogoria and Lake Naivasha, Kenya, Oct. 29 – Nov. 19, 2010. 3 p. Can be accessed at http://www.os.is/gogn/unu-gtp-sc/UNU-GTP-SC-11-21.pdf

Hockin, S.L. and G.M. Gadd, 2003. Linked redox-precipitation of sulfur and selenium under anaerobic conditions by sulfate-reducing bacterial biofilms. Appl Environ Microbiol 69, 7063–7072 p.

Hunt, R.J., D.P. Krabbenhoft and M.P. Anderson. 1996, Groundwater inflow measurements in wetland systems, Water Resources. Research, 32, doi:101029/95WR03724. 495-507 p.

Israelson, O.W. and R.C. Reeve. 1944, Canal lining experiments in the Delta Area, Utah. Utah Agricultural Experimental Station, Bulletin 313: 15-35 p.

Johnson, W. P., D. L. Naftz, X. Diaz, K. Beisner, and W. Oliver. 2008, Estimation of Selenium Removal Fluxes from the South Arm of the Great Salt Lake, Utah: Final Report. April 7.

Keimowitz, A. R.; Datta, S.; Stute, M.; Simpson, H. J.; Chillrud, S. N.; Tsang, M.; Ross, J. 2003, Arsenic mobilization under reducing conditions beneath a landfill in Maine., Abstracts of Papers of the American Chemical Society, Sep, Volume 226, 584-586 p.

Keller, G.V. and F.C. Frischknecht. 1966, Electrical methods in geophysical prospecting. Pergamon Press, 90-196 p.

Knudson, 2002. unpublished Undergrad research of Great Salt Lake chemistry. Written communication .

KUCC, Kennecott Utah Copper Corporation. 1999, Kennecott Utah Copper Corporation-North End Groundwater RI Report, 7.3 nature and extent of contamination. Unpublished report.

Lambert, P.M. 1995a, Numerical simulation of ground-water flow in basin-fill material in Salt Lake Valley, Utah: Utah Department of Natural Resources Technical Publication 110-B, 58 p.

Lambert, P.M. 1995b, Particle-tracking analysis of time-related capture zones for selected public-supply wells in Salt Lake Valley, Utah: Utah Department of Natural Resources Technical Publication 110-C, 36 p.

Landmeyer, J.E. 1996, Aquifer response to record low barometric pressures in Southeastern United States: Ground Water, v. 34, no. 5, 917– 924 p.

Lane, J.W., Jr. 2007, Using fiber-optic distributed temperature sensors to monitor ground-water and surface-water processes and interaction [abs.]: NGWA Ground Water Summit, Albuquerque, New Mexico, April 29 - May 30, 2007, Proceedings: Westerville, Ohio, National Ground Water Association.

Lee, D.R. 1977, A device for measuring seepage flux in lakes and estuaries. Limnology and Oceanography 22 (1), 140–147 p.

Maher, R C. 2006, Temperature-dependent antistokes/stokes ratios under surface-enhanced Raman scattering conditions. The journal of physical chemistry. B 110.132006: 6797-6803 p.

Manning, A. H., D. K. Solomon. 2003, Using noble gases to investigate mountain-front recharge. J. hydrol. 275, 194-207.

Merkel B., B. Planer-Friedrich , D. Kirk-Nordstrom. 2005, A Practical Guide To Modeling Of Natural And Contaminated Aquatic Systems, Volume 1. 20 p.

Mesowest. 2012, http://mesowest.utah.edu/index.html. Accessed February, 2012.

Miller, D. E.1980, Great Salt Lake: A Historical Sketch. Utah Geological and Mineral Survey. Bulletin 116,10 p.

Moffett, K. B. 2008, Processes controlling the thermal regime of saltmarsh channel beds." Environmental science and technology 42.32008: 671-676 p.

Mohammed, I. N., and D. G. Tarboton. 2011, On the interaction between bathymetry and climate in the system dynamics and preferred levels of the Great Salt Lake, Water Resources Research., 47, doi:10.1029/2010WR009561. 2-3 p.

Mower, R.W. 1968, Ground-water discharge toward Great Salt Lake through basin fill in the Jordan Valley, Utah, in Geological Survey research 1968: U.S. Geological Survey Professional Paper 600-D, D71-D74 p.

Naftz, D.L., W.P. Johnson,, M.L. Freeman, K. Beisner, X. Diaz, and Cross, V.A. 2008, Estimation of selenium loads entering the south arm of Great Salt Lake, Utah, from May 2006 through March 2008: U.S.Geological Survey Scientific Investigations Report 2008–5069, 40 p.

Naftz, D.L., C. Angeroth, , T. Kenney, B. Waddell, S. Silva, N. Darnall, C. Perschon, and J. Whitehead. 2008, Anthropogenic influences on the input and biogeochemical cycling of nutrients and mercury in Great Salt Lake, Utah, USA: Applied Geochemistry, vol. 23, p. 1731–1744.

Palluconi, F.D. and G.R. Meeks. 1985, Thermal-Infrared ultispectral-Scanner (TIMS)-An investigator's guide to TIMS data. Pasadena CA, National Aeronautics and Space administration, Jet Propulsion Lan Publication 85-32, 25 p.

Plummer, L. N., D.L. Parkhurst, G.W. Fleming, S.A. Dunkle. 1988, A computer program incorporating Pitzer's equations for calculation of geochemical reactions in brines. U.S. Geological Survey Water-Resources Investigations Report 88-4153, 310 p.

Révész, Kinga, and T.B. Coplen. 2008a, Determination of the δ(2H/1H) of water: RSIL lab code 1574, chap. C1 of Révész, Kinga, and T.B. Coplen, eds., Methods of the Reston Stable Isotope Laboratory: U.S.Geological Survey Techniques and Methods 10–C1, 27 p.

Révész, Kinga, and T.B. Coplen, 2008b, Determination of the δ(18O/16O) of water: RSIL lab code 489, chap. C2 of Révész, Kinga, and T.B. Coplen, eds., Methods of the Reston Stable Isotope Laboratory: U.S. Geological Survey Techniques and Methods, 10–C2, 28 p.

Révész, Kinga, and H. Qi. 2006, Determination of the δ(34S/32S) of Sulfate in Water: RSIL Lab Code 1951, chap. C10 of Révész, Kinga, and Coplen, Tyler B., eds., Methods of the Reston Stable Isotope Laboratory: Reston, Virginia, U.S. Geological Survey, Techniques and Methods, book 10, sec. C, chap. 10, 33 p.

Richardson, G.B. 1906, Underground water in the valleys of Utah Lake and Jordan River, Utah: U.S. Geological Survey Water Supply Paper 157, 81 p.

Roberts, W. C. 2010, Extracting Minerals from the Great Salt Lake: an Analysis of Barriers to Entry within the Market for Nutritional Minerals. University of Utah, work in progress. 3 P.

Rosenberry, D.O. 2008, A seepage meter designed for use in flowing water**:** Journal of Hydrology, vol. 359, 118-130 p.

Schlosser, P., Stute, M., Sonntag, C., and Munnich, K.O., 1988, Tritogenic ^{3}He in Shallow Groundwater. Earth and Planetary Science Letters, v. 89, pp. 353-362.

Schreiber, M.E., M.B. Gotkowitz, J.A. Simo, and P.G. Freiberg. 2003, Mechanisms of Arsenic Release to Ground Water from Naturally Occurring Sources, Eastern Wisconsin. In: A.H. Welch, and K.G. Stollenwerk (Editor), Arsenic in Ground Water: Geochemistry and Occurrence. Kluwer Academic Publishers, Norwell, Massachusetts, 259-280 p.

Shelly, K. 2010, Fact Sheet / Statement Of Basis Jordan Valley Water Conservancy District Southwest Groundwater Treatment Plant New Permit: Discharge Updes Permit Number: Ut0025836 Major Industrial. Can be accessed at http://www.deq.utah.gov/businesses/jordonvalleywater/index.htm

Smith, J.W.N. 2005, Groundwater-surface water interactions in the hyporheic zone. July 2005.Science report SC030155/SR1. Environment Agency. 17 p.

Solomon, D.K., and Cook, P.G., 2000, ^{3}H and ^{3}He, in Cook, P.G., and Herczeg, A.L., eds., Environmental tracers in subsurface hydrology: Boston, Kluwer Academic Publishers, 425–439 p.

Stephens, D. and P. W. Birdsey, Jr. 2002, Population dynamics of the brine shrimp, Artemia franciscana, in Great Salt Lake and Regulation of Commercial Shrimp Harvest. In Great Salt Lake: An Overview of Change, ed. J.

Stolp, B.J. and L.E. Brooks. 2009, Hydrology and simulation of ground-water flow in the Tooele Valley ground-water basin, Tooele County, Utah: U.S. Geological Survey Scientific Investigations Report 2009-5154, 86 p.

Stute, M., and Schlosser, P., 2001, Atmospheric noble gases, in Cook, P.G., and Herczeg, A.L., eds., Environmental tracers in subsurface hydrology: Boston, Kluwer Academic Publishers, 349–377 p.

Taylor, G.H., and R.H. Leggette. 1949, Ground water in JordanValley, Utah: U.S. Geological Survey Water Supply Paper 1029, 357 p.

Telford, W.M., Geldart, L.P., Sheriff, R.E. 1990, Applied Geophysics, 2nd ed. Cambridge: Cambridge University Press.

Thiros, S.A. 1992, Selected hydrologic data for Salt Lake Valley, Utah, 1990-92, with emphasis on data from the shallow unconfined aquifer and confining layers: U.S. Geological Survey Open-File Report 92-640, duplicated as Utah Hydrologic-Data Report No. 49, 44 p.

Thiros, S.A. 1995, Chemical composition of ground water, hydrologic properties of basin-fill material, and ground-water movement in Salt Lake Valley, Utah:Utah Department of Natural Resources Technical Publication No. 110-A, 59 p.

Thiros, S.A., L.M. Bexfield, D.W. Anning, and J.M. Huntingtoneds. 2010, Conceptual understanding and groundwater quality of selected basin-fill aquifers in the Southwestern United States: U.S. Geological Professional Paper 1781, 288 p.

U.S. Environmental Protection Agency. 1983, Methods for chemical analysis of water and wastes—Office of Research chemical analysis of water and wastes: Washington, D.C., Office of Research and Development Report EPA 600/4-79-020, 552 p.

U.S. Geological Survey. 2012a, http://ut.water.usgs.gov/. Accessed March, 2012.

U.S. Geological Survey. 2012b, variously dated, National field manual for the collection of water-quality data: U.S. Geological Survey Techniques of Water-Resources Investigations, book 9, chaps. A1-A9, available online at http://pubs.water.usgs.gov/twri9A.

U.S. Geological Survey. 2012c, http://waterdata.usgs.gov/ut/nwis/uv?site_no=10010000. Accessed February, 2012.

Utah gov. 2012, http://www.rules.utah.gov/publicat/bulletin/2012/20120215/35359.htm. Accessed March, 2012.

Waddell, K.M., R.L. Seiler, M. Santini, and D.K. Solomon. 1987, Ground-water conditions in Salt Lake Valley, Utah, 1969-83, and predicted effects of increased withdrawals from wells: Utah Department of Natural Resources Technical Publication No. 87, 69 p.

Watson, J.T. 1997, Introduction to Mass Spectrometry, 3rd Edition, Lippincott-Raven. Philidelphia, PA. 180-181 p.

Wilson, S.R. and F.L. Wideman. 1957, Sodium sulfate deposits along the southeast shore of Great Salt Lake. Salt Lake and Toole Counties, Utah: US Bureau of Mines Information Circular. No. 7773.United States Department Of Interior. 10 p.

Winter, T.C. 1981, Uncertainties in estimating the water balance of lakes. Water Resource Bulletin, 17, 82-115 p.

Wright, M.T., K. Belitz, and T. Johnson. 2004, Assessing the susceptibility to contamination of two aquifer systems used for public water supply in the Modesto and Fresno metropolitan areas, California, 2001 and 2002: U.S. Geological Survey Scientific Investigations Report 2004–5149, 1 p.